CRC Report No. A-139

Improving Modeled Biogenic VOC and Anthropogenic VCP Contributions to Organic Aerosol over the San Francisco Bay Area and Evaluating Emission Reductions

Final Report

February 2026

COORDINATING RESEARCH COUNCIL, INC.
1 CONCOURSE PARKWAY • SUITE 800 • ATLANTA, GA 30328

The Coordinating Research Council, Inc. (CRC) is a non-profit corporation supported by the petroleum and automotive equipment industries with participation from other industries, companies, and governmental bodies on research programs of mutual interest. CRC operates through the committees made up of technical experts from industry and government who voluntarily participate. The five main areas of research within CRC are: air pollution (atmospheric and engineering studies); aviation fuels, lubricants, and equipment performance; heavy-duty vehicle fuels, lubricants, and equipment performance (e.g., diesel trucks); light-duty vehicle fuels, lubricants, and equipment performance (e.g., passenger cars); and sustainable mobility (e.g., decarbonization). CRC's function is to provide the mechanism for joint research conducted by industries that will help in determining the optimum combination of products. CRC's work is limited to research that is mutually beneficial to the industries involved. The final results of the research conducted by, or under the auspices of, CRC are available to the public.

LEGAL NOTICE

This report was prepared by Ramboll as an account of work sponsored by the Coordinating Research Council (CRC). Neither the CRC, members of the CRC, Ramboll, nor any person acting on their behalf: (1) makes any warranty, express or implied, with respect to the use of any information, apparatus, method, or process disclosed in this report, or (2) assumes any liabilities with respect to use of, inability to use, or damages resulting from the use or inability to use, any information, apparatus, method, or process disclosed in this report. In formulating and approving reports, the appropriate committee of the Coordinating Research Council, Inc. has not investigated or considered patents which may apply to the subject matter. Prospective users of the report are responsible for protecting themselves against liability for infringement of patents.

Prepared for:

Coordinating Research Council (CRC)
1 Concourse Parkway Suite 800
Atlanta, GA 30328

Prepared by:

Ramboll Americas Engineering Solutions, Inc.
7250 Redwood Blvd., Suite 105
Novato, California 94945

September 2026
1940113060

CRC PROJECT A-139 FINAL REPORT

Improving Modeled Biogenic VOC and Anthropogenic VCP Contributions to Organic Aerosol over the San Francisco Bay Area and Evaluating Emission Reductions

This technical report was prepared with support from the Bay Area Air District (District). The opinions, findings, conclusions, and recommendations expressed herein are those of the authors and do not necessarily reflect the views of the District. The District, its officers, employees, contractors, and subcontractors make no warranty, expressed or implied, and assume no legal liability for the information in this report.

RAMBOLL Bright ideas. Sustainable change.

CRC PROJECT A-139 FINAL REPORT
IMPROVING MODELED BIOGENIC VOC AND ANTHROPOGENIC VCP CONTRIBUTIONS TO ORGANIC AEROSOL OVER THE SAN FRANCISCO BAY AREA AND EVALUATING EMISSION REDUCTIONS

Ramboll
7250 Redwood Boulevard
Suite 105
Novato, CA 94945
USA

T +1 415 899 0700
https://ramboll.com

CONTENTS

List of Acronyms and Abbreviations **4**
Executive Summary **5**
1.0 Introduction **7**
2.0 Model Updates **8**
2.1 VCP Chemistry Implementation in SAPRC-22 8
2.1.1 New SAPRC-22-VCP reactions 8
2.1.2 Removing VCPs from SAPRC-22 lumped alkanes 12
2.1.3 SOA production from VCPs and large alkanes 15
2.2 Other SOA Updates 15
2.2.1 SOA production from IVOC and aromatics 15
2.2.2 SOA production from BVOCs 18
3.0 Base Case Modeling **23**
3.1 Model Setup 23
3.2 Model Emissions 24
3.2.1 Anthropogenic emissions for SAPRC-22 and SAPRC-22-VCP simulations 25
3.2.2 SAPRC-22 vs SAPRC-22-VCP SOA forming potential of precursors 26
3.2.3 Biogenic emissions 28
3.3 Model Performance for $PM_{2.5}$ 36
3.3.1 Model Performance for Total $PM_{2.5}$ 36
3.3.2 Model Performance for Speciated $PM_{2.5}$ 40
3.3.3 Discussion of model performance 40
4.0 Emission Scenarios **48**
5.0 Conclusions and Recommendations **59**
6.0 References **60**

Table of Figures

Figure 3-1. The Air District CMAQ modeling domains. 24
Figure 3-2. Total SOA potential and contribution of SOA precursor species for SAPRC-22 and SAPRC-22-VCP. 27
Figure 3-3. Emissions of anthropogenic SOA precursor species within the Air District's 1-km regional modeling domain for SAPRC-22 and SAPRC-22-VCP. 28
Figure 3-4. Differences between total MEGAN and BEIS emissions (in moles) of α-pinene in July 2022. 31
Figure 3-5. Differences between total MEGAN and BEIS emissions (in moles) of β-pinene in July 2022. 32
Figure 3-6. Differences between total MEGAN and BEIS emissions (in moles) of isoprene in July 2022. 33

Figure 3-7. Differences between total MEGAN and BEIS emissions (in moles) of sesquiterpenes in July 2022. 34
Figure 3-8. Differences between total MEGAN and BEIS emissions (in moles) of other terpenes in July 2022. 35
Figure 3-9. Locations of the Air District's PM monitoring sites within its jurisdiction, shown by the black outline that generally follows the 9-county boundaries. The Bay Area 1 km grid is indicated by the red box. 37
Figure 3-10. Soccer plots of $PM_{2.5}$ model performance by month (across all sites) for (a) SAPRC07-AERO7-MEGAN, (b) SAPRC-22-AERO68-BEIS, (c) SAPRC-22-VCP-AERO68-BEIS, and (d) SAPRC-22-VCP-AERO68-MEGAN. 38
Figure 3-11. Soccer plots of annual $PM_{2.5}$ model performance by monitoring site for (a) SAPRC07-AERO7-MEGAN, (b) SAPRC-22-AERO68-BEIS, (c) SAPRC-22-VCP-AERO68-BEIS, and (d) SAPRC-22-VCP-AERO68-MEGAN. 39
Figure 3-12. NMB in seasonal and annual $PM_{2.5}$ sulfate at the San Jose-Jackson CSN monitor for (a) SAPRC07-AERO7-MEGAN, (b) SAPRC-22-AERO68-BEIS, (c) SAPRC-22-VCP-AERO68-BEIS, and (d) SAPRC-22-VCP-AERO68-MEGAN. 41
Figure 3-13. NMB in seasonal and annual $PM_{2.5}$ nitrate at the San Jose-Jackson CSN monitor for (a) SAPRC07-AERO7-MEGAN, (b) SAPRC-22-AERO68-BEIS, (c) SAPRC-22-VCP-AERO68-BEIS, and (d) SAPRC-22-VCP-AERO68-MEGAN. 42
Figure 3-14. NMB in seasonal and annual $PM_{2.5}$ organic carbon at the San Jose-Jackson CSN monitor for (a) SAPRC07-AERO7-MEGAN, (b) SAPRC-22-AERO68-BEIS, (c) SAPRC-22-VCP-AERO68-BEIS, and (d) SAPRC-22-VCP-AERO68-MEGAN. 43
Figure 3-15. Monthly average MDA8 ozone in January: SAPRC07 chemistry (left), SAPRC-22 chemistry (middle), SAPRC-22 – SAPRC07 (right). 44
Figure 3-16. Monthly average MDA8 ozone in April: SAPRC07 chemistry (left), SAPRC-22 chemistry (middle), SAPRC-22 – SAPRC07 (right). 45
Figure 3-17. Monthly average MDA8 ozone in July: SAPRC07 chemistry (left), SAPRC-22 chemistry (middle), SAPRC-22 – SAPRC07 (right). 46
Figure 4-1. January average $PM_{2.5}$ anthropogenic SOA and responses to emissions reductions. 49
Figure 4-2. January average $PM_{2.5}$ biogenic SOA and responses to emissions reductions. 51
Figure 4-3. January average $PM_{2.5}$ organic carbon (OC) mass and responses to emissions reductions. 52
Figure 4-4. January average $PM_{2.5}$ nitrate and responses to emissions reductions. 53
Figure 4-5. January average $PM_{2.5}$ ammonium and responses to emissions reductions. 54
Figure 4-6. January average total $PM_{2.5}$ and responses to emissions reductions. 55
Figure 4-7. April average total $PM_{2.5}$ and responses to emissions reductions. 57
Figure 4-8. July average total $PM_{2.5}$ and responses to emissions reductions. 58

Table of Tables

Table 2-1. VCP species for alcohols, ethers, esters and siloxanes added to SAPRC-22. 9

Table 2-2. Reactions of VCP species for alcohols, ethers, esters and siloxanes added to SAPRC-22. 10

Table 2-3. Contributions of VCP compounds (% by mass) to SAPRC-22 lumped alkane species. 12

Table 2-4. Revised reactions of SAPRC-22 lumped alkanes ALK3 to ALK6 with contributions of VCP compounds removed. 13

Table 2-5. Reactions added to SAPRC-22 to better represent SOA production from VCPs and large alkanes. 16

Table 2-6. New RO_2 species added to SAPRC-22 to represent SOA production from VCPs and large alkanes. 16

Table 2-7. Reactions updated or added to SAPRC-22 to better represent SOA production from IVOC and aromatics. 17

Table 2-8. New species added to SAPRC-22 to better represent SOA production from IVOC and aromatics. 18

Table 2-9. New organic nitrate species from terpene precursors in modified SAPRC-22. 20

Table 2-10. Terpene reactions with NO_3 radicals in the modified SAPRC-22 mechanism. 20

Table 2-11. New reactions added to SAPRC-22 to represent terpene organic nitrate chemistry. 21

Table 3-1. Base case CMAQ simulations. 23

Table 3-2. SAPRC-22 emissions (tons/day) for each sector, summed across all counties. 25

Table 3-3. SAPRC-22-VCP emissions (tons/day) for each sector, summed across all counties 26

Table 3-4. Anthropogenic SOA precursors and SOA yields. 26

Table 3-5. BEIS estimates of monthly and annual average biogenic species emissions (tons/day) over the 1 km modeling domain. 29

Table 3-6. MEGAN estimates of monthly and annual average biogenic species emissions (tons/day) over the 1 km modeling domain. 30

Table 4-1. List of $PM_{2.5}$ variables provided for analysis. 48

LIST OF ACRONYMS AND ABBREVIATIONS

BCs	Boundary Conditions
BEIS	Biogenic Emission Inventory System
BVOC	Biogenic VOCs
CARB	California Air Resources Board
CEPAM	California Emissions Projection Analysis Model
CERP	Community Emissions Reduction Plans
CMAQ	Community Multiscale Air Quality model
CRC	Coordinating Research Council
EMFAC	EMission FACtor
EPA	Environmental Protection Agency
FEM	Federal Equivalent Methods
FRM	Federal Reference Methods
ICs	Initial Conditions
IVOC	Intermediate volatility VOC
LAI	Leaf Area Index
MCIP	Meteorology-Chemistry Interface Program
MDA8	Maximum Daily 8-hour Average
MEGAN	Model of Emissions of Gases and Aerosols from Nature
NMB	Normalized Mean Bias
NME	Normalized Mean Error (unsigned, or gross)
OA	Organic Aerosol
OC	Organic Carbon
NOx	Nitrogen oxides
$PM_{2.5}$	Particulate Matter less than 2.5 microns
SAPRC	Statewide Air Pollution Research Center
SMOKE	Sparse Matrix Operator Kernel Emissions
SOA	Secondary Organic Aerosol
VCP	Volatile Chemical Products
VOC	Volatile organic compounds
WACCM	Whole Atmosphere Community Climate Model
WRF	Weather Research and Forecasting model

EXECUTIVE SUMMARY

This collaborative study was conducted under the joint sponsorship of CRC and the Bay Area Air District (also referred to as the "Air District" in this report) to improve $PM_{2.5}$ modeling in the San Francisco Bay Area. As part of the study, Ramboll updated the recently developed SAPRC-22 chemistry version of CMAQ to include VCP chemistry and updated the treatment of secondary organic aerosols.

VCP Updates

Volatile chemical products (VCPs) comprise a substantial and growing fraction of anthropogenic VOC emissions in the US. Many VCP compounds are engineered to have desirable physical properties when used in chemical products (e.g., solvents, cleaners, paints, personal care products), making them chemically different from many traditional VOCs that are obtained directly from crude oil.

We added chemical species and reactions to the SAPRC-22 chemical mechanism to better represent VCP alcohols, ethers, glycol ethers, esters and siloxanes. To avoid duplication, we also revised the SAPRC-22 reactions of lumped alkane species (ALK3, ALK4, ALK5 and ALK6) to remove large (31% to 48% by mass) contributions of oxygenated VCPs that were assumed in the derivation of the chemical reactions of ALK3 to ALK6. Finally, we added chemistry to represent SOA formation from some VCPs. We refer to this version of SAPRC-22 as SAPRC-22-VCP.

Other SOA Updates

Oxidation of intermediate volatility organic compounds (IVOC) and aromatics can lead to SOA formation. We added IVOC chemistry and updated aromatic reactions in SAPRC-22 and SAPRC-22-VCP to better represent SOA production from these species.

We added the production of isoprene epoxydiols (IEPOX), to the isoprene chemistry in SAPRC-22 to form SOA via heterogeneous uptake to aerosols. We also updated the terpene chemistry to add production of terpene-specific organic nitrates that can then form SOA via heterogeneous uptake and hydrolysis.

Species Mappings for Emissions and ICs/BCs

Ramboll developed speciation mappings for SMOKE to support the SAPRC-22 and SAPRC-22-VCP simulations. Speciation mapping refers to translating the detailed VOC compounds present in VOC speciation profiles to the VOC model species used by condensed chemical mechanisms such as SAPRC-22. We first developed mappings for VOCs in EPA's SPECIATE (version 5.3) profiles to process SAPRC-22 species, following assignments from the chemical speciation database SpecDB (Carter, 2015). The SAPRC-22 mappings were then updated to include VCP model species by first mapping the explicit VCPs in SAPRC-22-VCP, mapping the lumped siloxanes to model species SXD5, and then assigning lumped oxygenates with the priority of ethers (ETHR) > alcohols (ROH) > esters (ESTR).We ran Ramboll's Speciation Tool to create SMOKE-ready VOC speciation profiles for both SAPRC-22 and SAPRC-22-VCP, generating a total of 2,676 profiles from SPECIATE5.3. These profiles were provided to the Air District who ran SMOKE.

Ramboll provided species mappings for SAPRC-22 with and without VCPs to the Air District to facilitate creation of initial and boundary conditions (ICs/BCs)

Base Case Simulations

The Air District conducted 3 annual base case simulations for calendar year 2022. The 3 base case simulations included different combinations of chemistry (SAPRC-22 and SAPRC-22-VCP) and biogenic emissions (BEIS and MEGAN).

The Air District provided the model performance evaluation results for $PM_{2.5}$ to Ramboll for review. As a reference point for comparison, the Air District also provided results from its most recent modeling platform using CMAQ with SAPRC07 chemistry and MEGAN biogenic emissions.

The model performance evaluation for total $PM_{2.5}$ over all monitoring locations within the Air District's jurisdiction and speciated $PM_{2.5}$ at a single CSN monitor showed that using SAPRC-22 chemistry improved model performance in spring by reducing the under-prediction bias, but worsened performance in winter by increasing the over-prediction bias. In general, the results show that the SAPRC-22 chemistry mechanism tends to be more conducive to oxidant formation, particularly in winter, than the SAPRC07 chemistry mechanism used in prior Air District CMAQ applications. This is confirmed by a comparison of ozone concentrations from the SAPRC07 and SAPRC-22 simulations.

Including VCP chemistry and using MEGAN emissions instead of BEIS emissions had a negligible effect on model performance. Nevertheless, the VCP updates to CMAQ represent an improvement to the model as the importance of VCP chemistry has been noted by a number of researchers (e.g., McDonald et al., 2018; Zhu et al., 2024; Stockwell et al., 2025).

While the over-prediction bias in $PM_{2.5}$ predictions in winter worsened when using SAPRC-22 chemistry, this could be related to uncertainties in the emission inventory, particularly the VOC inventory. Other sources of uncertainty include the boundary conditions from WACCM.

Emission Reduction Scenario Simulations

The Air District conducted 4 monthly emission scenario model simulations for 3 months representing the winter, summer, and spring/fall seasons. The scenarios included:

1. 20% anthropogenic VOC reduction
2. 40% anthropogenic VOC reduction
3. 40% anthropogenic NOx reduction
4. 40% anthropogenic NOx and VOC reduction

Results from the emission reduction scenario simulations showed that some portions of the Bay Area are likely VOC-limited, since NOx reductions resulted in increases in anthropogenic and biogenic SOA. Responses to emission reductions were larger in the winter month than in either the spring month or the summer month. Both VOC and NOx reductions are required to decrease total $PM_{2.5}$.

Recommendations

We recommend the following for future work:

- Conduct a robust assessment of anthropogenic emissions inventory (both VOCs and NOx)
- Assess VCP emissions inventory
- Add more speciated ($PM_{2.5}$, VOCs) monitoring sites

1.0 INTRODUCTION

This report describes a collaborative study co-funded by the Coordinating Research Council (CRC) and the Bay Area Air District (aka Air District) to improve fine particulate matter ($PM_{2.5}$) modeling in the San Francisco Bay Area. The Air District uses the U.S. Environmental Protection Agency's (EPA) Community Multiscale Air Quality (CMAQ) model[1,2] to characterize ambient fine particulate matter ($PM_{2.5}$) concentrations across the Bay Area. Such modeling supports various Air District programs including planning, rule development, and Community Emissions Reduction Plans (CERPs) under Assembly Bill 617[3]. The CMAQ domain features a horizontal grid network of 1 km cells covering the entire Bay Area, and a vertical structure with 28 model layers extending through the entire troposphere.

In recent applications conducted by the Air District, CMAQ was found to overestimate $PM_{2.5}$ concentrations during winter months and underestimate during spring months. Organic aerosol (OA) comprises a large fraction of $PM_{2.5}$ concentrations in the Bay Area with contributions from local and regional biogenic and anthropogenic VOC emissions. Uncertainties in emissions and chemistry (oxidation and volatility) of these VOCs are believed to contribute to the underpredictions of organic carbon during the warmer months. Secondary organic aerosols (SOA) from biogenic VOCs (BVOCs) can be a large fraction of $PM_{2.5}$ mass (e.g., Pfannerstill et al., 2024) and uncertainties in BVOC emissions can lead to inaccuracies in model predictions. Urban BVOC emissions are challenging to estimate because vegetative cover constantly evolves with urban development and urban tree species may differ from the natural ecosystem in ways that are often poorly characterized.

Similarly, detailed VOC measurements show that volatile chemical products (VCPs), such as personal care items, paints, and cleaning agents, are becoming the dominant anthropogenic VOC source (McDonald et al., 2018) in many regions. Air quality planning must look beyond reducing conventional VOC emission categories to achieve effective attainment strategies. VCP compounds are chemically diverse with widely-varying potentials to form ozone and SOA. Models need detailed VCP oxidant chemistry (Yarwood and Tuite, 2024) that is integrated with SOA chemistry for anthropogenic VOC and intermediate volatility VOC (IVOC) compounds.

To address these limitations in their current modeling platform, the Air District adopted two concurrent approaches:

1. The Air District updated urban BVOC emissions by using satellite, aerial, and other data processed by machine learning with methods pioneered by the University of California, Irvine (UCI) and Ramboll (Guenther et al., 2019) to improve BVOC emission estimates from the Model of Emissions of Gases and Aerosols from Nature (MEGAN). The updated BVOC emissions were used by the Air District in some of the simulations conducted in this study.

2. Ramboll, under joint funding from CRC and the Air District, updated CMAQ with the latest version of the SAPRC gas-phase chemistry (SAPRC-22)[4] coupled with new VCP chemistry, updated organic aerosol chemistry, and improved organic emission inventories. The Air District conducted CMAQ simulations with the updated modeling platform and provided the results to Ramboll for analysis. This work is described in this report.

[1] https://www.epa.gov/cmaq
[2] https://github.com/USEPA/CMAQ/blob/main/DOCS/Users_Guide/README.md
[3] https://www.baaqmd.gov/community-health/community-health-protection-program
[4] https://intra.cert.ucr.edu/~carter/SAPRC/22/

2.0 MODEL UPDATES

The Air District uses the U.S. EPA's CMAQ model to simulate and predict regional levels of ozone and fine particulate matter ($PM_{2.5}$) for forecasting and planning and policy evaluation. Gas-phase photochemistry in CMAQ is simulated using the Statewide Air Pollution Research Center 2007 (SAPRC07) mechanism expanded to include certain toxics (SAPRC07TC). Aerosol chemistry is simulated using the EPA AERO7 mechanism. In an EPA-sponsored study, Ramboll (Karamchandani et al., 2025) recently implemented the latest version of the SAPRC mechanism, referred to as SAPRC-22 (Carter, 2023), in CMAQ. This version of CMAQ is available on the U.S. EPA's CMAQ GitHub site[5], and was used as the starting point for the study described here. Below, we describe the updates that were made to the model for the CRC-Air District collaborative study.

2.1 VCP Chemistry Implementation in SAPRC-22

Volatile chemical products (VCPs) comprise a substantial and growing fraction of anthropogenic VOC emissions in the US. Many VCP compounds are engineered to have desirable physical properties when used in chemical products (e.g., solvents, cleaners, paints, personal care products), making them chemically different from many traditional VOCs that are obtained directly from crude oil.

We added chemical species and reactions to the SAPRC-22 chemical mechanism to better represent VCP alcohols, ethers, glycol ethers, esters and siloxanes. To avoid duplication, we also revised the SAPRC-22 reactions of lumped alkane species (ALK3, ALK4, ALK5 and ALK6) to remove large (31% to 48% by mass) contributions of oxygenated VCPs that were assumed in the derivation of the chemical reactions of ALK3 to ALK6. Finally, we added chemistry to represent SOA formation from some VCPs. We refer to this version of SAPRC-22 as SAPRC-22-VCP. The specific updates made to develop SAPRC-22-VCP are described below.

2.1.1 New SAPRC-22-VCP reactions

Table 2-1 lists the species that were added to SAPRC-22 to represent alcohols, ethers, esters and siloxanes. These model species correspond with those in the VCP mechanism from Yarwood and Tuite (2024), except that glycerol is a new addition. As described in Yarwood and Tuite (2024), the new model species were developed following analysis of a U.S.-wide VCP emission inventory (Seltzer et al., 2021) to identify VCP compounds that are most important to ozone and SOA formation. We added reactions of these VCP species with OH-radical to SAPRC-22 as shown in Table 2-2. We omitted reactions with other oxidants (NO_3, O_3) and photolysis because they are too slow to compete with the OH-reaction and/or deposition removal. We derived the reaction mechanisms and rate constants using the MechGen software (Carter et al., 2025) that was also used to develop the base SAPRC-22 mechanism (Carter, 2023) and is accessible at https://intra.engr.ucr.edu/~carter/MechGen/.

Temperature-dependent rate constants are specified using a modified Arrhenius expression:

$$kT = A\ T^{n}\ \exp(-E_a/T)$$

where A is the Arrhenius parameter (cm^{-3} $molec^{-1}$ s^{-1}), T is the temperature (K) and E_a is the activation energy (K).

[5] https://github.com/USEPA/CMAQ/blob/5.4_SAPRC22/README.md

Table 2-1. VCP species for alcohols, ethers, esters and siloxanes added to SAPRC-22.

SAPRC-22-VCP Species Name	Explicit or Lumped	Representing
ETGLYCL	Explicit	ethylene glycol
PRGLYCL	Explicit	propylene glycol
IC3OH	Explicit	i-propanol
NC3OH	Explicit	n-propanol
GLYCERL	Explicit	glycerol
ROH	Lumped	lumped alcohols except for explicit alcohols
MEOME	Explicit	dimethyl ether
ETOET	Explicit	diethyl ether
ETHR	Lumped	lumped ethers except for explicit ethers
MEFORM	Explicit	methyl formate
MEACET	Explicit	methyl acetate
ETFORM	Explicit	ethyl formate
ETACET	Explicit	ethyl acetate
ESTR	Lumped	lumped esters except for explicit esters
SXD5	Lumped	lumped siloxanes based on D5-siloxane

Table 2-2. Reactions of VCP species for alcohols, ethers, esters and siloxanes added to SAPRC-22.

Reaction label	Reaction	A (cm^{-3} $molec^{-1}$ s^{-1})	E_a (K)	n	k_{298} (cm^{-3} $molec^{-1}$ s^{-1})[a]
VCP1	ETGLYCL + OH = HO2 + 0.06*HCHO + 0.97*GLCHO	1.45E−11			1.45E−11
VCP2	PRGLYCL + OH = 0.95*HO2 + 0.05*xHO2 + 0.05*RO2C + 0.03*HCHO + 0.05*xHCHO + 0.03*MECHO + 0.32*RCHO + 0.05*xGLCHO + 0.61*KET2 + 0.05*yROOH + 0.05*SumRO2 + 0.5*ETHRRO2	2.10E−11			2.10E−11
VCP3	IC3OH + OH = 0.85*HO2 + 0.15*xHO2 + 0.15*RO2C + 0.15*xHCHO + 0.15*xMECHO + 0.85*ACET + 0.15*yROOH + 0.15*SumRO2	7.21E−13	−594	1.41	5.24E−12
VCP4	NC3OH + OH = 0.58*HO2 + 0.41*xHO2 + 0.41*RO2C + 0.01*RO2XC + 0.39*xHCHO + 0.39*xMECHO + 0.58*ETCHO + 0.02*xRCHO + 0.01*zRHNO3 + 0.42*yROOH + 0.42*SumRO2	9.98E−13	−531	1.86	5.86E−12
VCP5	GLYCERL + OH = HO2 + 0.03*HCHO + 0.49*RCHO + 0.03*GLCHO + 0.48*KET2	1.22E−11			1.22E−11
VCP6	ROH + OH = 0.37*HO2 + 0.58*xHO2 + 0.62*RO2C + 0.04*RO2XC + 0.40*xHCHO + 0.19*xMECHO + 0.13*xETCHO + 0.04*xRCHO + 0.28*xACET + 0.06*xMEK + 0.02*xKET2 + 0.01*xGLCHO + 0.23*RCHO + 0.06*MEK + 0.08*KET2 + 0.04*zRHNO3 + 0.67*yROOH + 0.67*SumRO2	4.16E−12	−250		9.63E−12
VCP7	MEOME + OH = xHO2 + RO2C + 0.6*yROOH + MEFORM + SumRO2	1.02E−12	−308	2.09	2.83E−12
VCP8	ETOET + OH = 0.1*xHO2 + 0.97*RO2C + 0.05*RO2XC + 0.85*xMEO2 + 0.02*xHCHO + 0.05*zR2NO3 + 1.14*yROOH + 0.95*ETFORM + 1.87*SumRO2	4.21E−13	−1020	2.72	1.27E−11
VCP9	ETHR + OH = 0.16*HO2 + 0.51*xHO2 + 0.92*RO2C + 0.08*RO2XC + 0.25*xHCHO + 0.25*xMEO2 + 0.02*xRCHO + 0.09*xETCHO + 0.01*xKET2 + 0.16*RCHO + 0.65*ESTR + 0.03*zRHNO3 + 0.04*zR1NO3 + 0.69*yROOH + SumRO2 + ETHRRO2	1.13E−11	−80		1.48E−11
VCP10	MEFORM + OH = 0.54*xHO2 + 0.54*RO2C + 0.46*MECO3 + 0.26*xHCOOH + 0.32*yHPCRB + 0.28*ALK1 + 0.26*CO + 0.54*SumRO2 + 0.46*SumRCO3	2.68E−14	−568	3.76	1.76E−13
VCP11	MEACET + OH = 0.96*xHO2 + 0.97*RO2C + 0.03*RO2XC + 0.01*xMECO3 + 0.01*xHCHO + 0.09*xMGLY + 0.43*xOACID + 0.03*zRCNO3 + 0.62*yHPCRB + 0.43*CO + SumRO2 + 0.01*SumRCO3	6.05E−15	−1205	4.47	3.35E−13
VCP12	ETFORM + OH = 0.18*xHO2 + 1.04*RO2C + 0.03*RO2XC + 0.01*xMEO2 + 0.69*xMECO3 + 0.09*R2CO3 + 0.16*xHCHO + 0.02*xRCHO + 0.77*xHCOOH + 0.03*zRCNO3 + 0.73*yHPCRB + 0.09*ALK1 + 0.08*CO + 1.08*SumRO2 + 0.78*SumRCO3	8.10E−14	−713	2	8.75E−13

Reaction label	Reaction	A (cm^{-3} $molec^{-1}$ s^{-1})	E_a (K)	n	k_{298} (cm^{-3} $molec^{-1}$ s^{-1})[a]
VCP13	ETACET + OH = 0.1*xHO2 + 0.95*RO2C + 0.05*RO2XC + 0.01*xMEO2 + 0.84*xMECO3 + 0.01*xHCHO + 0.08*xRCHO + 0.43*xOACID + 0.03*zRCNO3 + 0.62*yHPCRB + 0.43*CO + SumRO2 + 0.01*SumRCO3	1.69E−13	−683		1.67E−12
VCP14	ESTR + OH = 0.40*xHO2 + 1.30*RO2C + 0.10*RO2XC + 0.13*xMEO2 + 0.23*xETO2 + 0.04*xMECO3 + 0.09*xR2CO3 + 0.03*xHCHO + 0.16*xMECHO + 0.08*xETCHO + 0.04*xRCHO + 0.13*xACET + 0.02*xKET2 + 0.08*xHCOOH + 0.17*xOACID + 0.02*R2CO3 + 0.12*CO + 0.08*ALK1 + 0.10*zRCNO3 + 1.07*yHPCRB + 0.09*yROOH + 1.40*SumRO2 + 0.02*SumRCO3	7.40E−13	−480		3.70E−12
VCP15	SXD5 + OH = 0.5*HCHO + 0.5*HCOOH + xHO2 + RO2C + yROOH + SumRO2 + SILXRO2	2.10E−12			2.10E−12

[a] k_{298} is the rate constant at 298 K and 1 atmosphere.

2.1.2 Removing VCPs from SAPRC-22 lumped alkanes

We revised the SAPRC-22 reactions of lumped alkane species (ALK3, ALK4, ALK5 and ALK6) to remove contributions of oxygenated VCPs that were assumed in the derivation of their chemical reactions (Table 2-3). The revised reactions of ALK3 to ALK6 with VCP contributions removed are shown in Table 2-4. Table 2-4 also includes the original reactions that were replaced.

Table 2-3. Contributions of VCP compounds (% by mass) to SAPRC-22 lumped alkane species.

SAPRC-22 Lumped Alkane	% VCP by mass[a]	VCP compounds built into each lumped alkane
ALK3	48%	Dimethyl ether, Propyl acetate
ALK4	31%	Isopropanol
ALK5	34%	Ethylene glycol, Propylene glycol, Glycerol, Butoxy ethanol
ALK6	45%	Texanol, Dipropylene glycol n-butyl ether

[a] Based on model species definition; not location-dependent.

Table 2-4. Revised reactions of SAPRC-22 lumped alkanes ALK3 to ALK6 with contributions of VCP compounds removed.

Reaction label	Revised/ Original	Reaction	A (cm^{-3} $molec^{-1}$ s^{-1})	E_a (K)	n	k_{298} (cm^{-3} $molec^{-1}$ s^{-1})[a]
L3OH	Revised	ALK3 + OH = 0.19*xHO2 + 1.24*RO2C + 0.17*RO2XC + 0.63*xTBUO + 0.20*xHCHO + 0.15*xRCHO + 0.14*xACET + 0.02*xKET2 + 0.05*zRHNO3 + 0.15*z1RNO3 + 1.41*yROOH + 1.41*SumRO2	3.9E−12	140		2.44E−12
L3OH	Original	ALK3 + OH = 0.34*xHO2 + 1.2*RO2C + 0.12*RO2XC + 0.14*xETO2 + 0.07*xR2CO3 + 0.33*xTBUO + 0.1*xHCHO + 0.1*xMECHO + 0.09*xRCHO + 0.07*xACET + 0.01*xKET2 + 0.12*xOACID + 0.07*zR1NO3 + 0.03*zRCNO3 + 0.02*zRHNO3 + 0.81*yROOH + 0.33*yHPCRB + 0.12*ALK1 + 16.91*NROG + 0.05*CO + 1.32*SumRO2	2.85E-12			2.85E-12
L4OH	Revised	ALK4 + OH = 0.01*xOH + 0.01*HO2 + 0.45*xHO2 + 1.33*RO2C + 0.17*RO2XC + 0.33*xETO2 + 0.02*xHCHO + 0.12*xMECHO + 0.07*xETCHO + 0.10*xRCHO + 0.44*xACET + 0.04*xMEK + 0.22*xKET2 + 0.13*zR1NO3 + 0.04*zRHNO3 + 1.46*yROOH + 0.01*HPCRB + 0.01*yHPCRB + 0.01*CO2 + 1.83*SumRO2	5.59E−12	−220		1.17E−11
L4OH	Original	ALK4 + OH = 0.01*xOH + 0.27*HO2 + 0.36*xHO2 + 0.96*RO2C + 0.12*RO2XC + 0.23*xETO2 + 0.06*xHCHO + 0.13*xMECHO + 0.05*xETCHO + 0.07*xRCHO + 0.26*ACET + 0.3*xACET + 0.03*xMEK + 0.15*xKET2 + 0.09*zR1NO3 + 0.03*zRHNO3 + 1.05*yROOH + 0.01*HPCRB + 0.01*yHPCRB + 0.01*CO2 + 1.08*SumRO2	4.54E-12			4.54E-12
L5OH	Revised	ALK5 + OH = ALK5_OH + 0.45*xHO2 + 1.44*RO2C + 0.31*RO2XC + 0.03*xETO2 + 0.02*xR2CO3 + 0.02*xHCHO + 0.05*xMECHO + 0.06*xRCHO + 0.02*xGLCHO + 0.08*xACET + 0.08*xMEK + 0.35*xKET2 + 0.02*xPACID + 0.12*zR1NO3 + 0.08*zR2NO3 + 0.03*zRCNO3 + 0.08*zRHNO3 + 1.53*yROOH + 0.18*yHPCRB + 1.78*SumRO2 + 0.02*SumRCO3 + 0.5*ALK6RO2	5.28E−12	−30		5.84E−12
L5OH	Original	ALK5 + OH = ALK5_OH + 0.3*HO2 + 0.33*xHO2 + RO2C + 0.22*RO2XC + 0.02*xETO2 + 0.01*xR2CO3 + 0.01*HCHO + 0.03*xHCHO + 0.04*xMECHO + 0.02*xETCHO + 0.11*RCHO + 0.04*xRCHO + 0.06*GLCHO + 0.01*xGLCHO + 0.05*xACET + 0.05*xMEK + 0.13*KET2 + 0.23*xKET2 + 0.01*xPACID + 0.08*zR1NO3 + 0.05*zR2NO3 + 0.02*zRCNO3 + 0.06*zRHNO3 + 1.05*yROOH + 0.12*yHPCRB + 0.01*ALK4 + 0.01*ALK5 + 1.22*SumRO2	1.14E-11			1.14E-11
597	Revised	ALK5_OH = 0.11*HO2 + 0.03*PACID + 0.08*HPCRB	1.94E-01			1.94E-01

Reaction label	Revised/ Original	Reaction	A (cm^{-3} $molec^{-1}$ s^{-1})	E_a (K)	n	k_{298} (cm^{-3} $molec^{-1}$ s^{-1})[a]
597	Original	ALK5_OH = 0.11*HO2 + 0.03*PACID + 0.08*HPCRB	2.87E-01			2.87E-01
598	Revised	ALK5_OH + NO = NO + 0.06*xHO2 + 0.11*RO2C + 0.02*RO2XC + 0.02*xMECO3 + 0.01*xR2CO3 + 0.02*xETCHO + 0.06*xRCHO + 0.01*xKET2 + 0.01*zRCNO3 + 0.01*zRHNO3 + 0.05*yROOH + 0.08*yHPCRB + 0.01*ALK5 + 0.12*SumRO2 + 0.01*SumRCO3	2.55E-12	-380		9.13E-12
598	Original	ALK5_OH + NO = NO + 0.06*xHO2 + 0.11*RO2C + 0.02*RO2XC + 0.02*xMECO3 + 0.01*xR2CO3 + 0.02*xETCHO + 0.06*xRCHO + 0.01*xKET2 + 0.01*zRCNO3 + 0.01*zRHNO3 + 0.05*yROOH + 0.08*yHPCRB + 0.01*ALK5 + 0.12*SumRO2	2.55E-12	-380		9.13E-12
L6OH	Revised	ALK6 + OH = ALK6_OH + 0.13*HO2 + 0.48*xHO2 + 1.03*RO2C + 0.50*RO2XC + 0.02*xR2CO3 + 0.02*xTBUO + 0.10*xHCHO + 0.13*RCHO + 0.15*xRCHO + 0.27*xACET + 0.47*xKET2 + 0.02*zR1NO3 + 0.23*zR2NO3 + 0.06*zRCNO3 + 0.19*zRHNO3 + 1.74*yROOH + 0.31*yHPCRB + 1.53*SumRO2 + 0.02*SumRCO3 + ALK6RO2	1.43E−11			1.43E−11
L6OH	Original	ALK6 + OH = ALK6_OH + 0.16*HO2 + 0.4*xHO2 + 0.97*RO2C + 0.33*RO2XC + 0.01*xR2CO3 + 0.01*xTBUO + 0.08*xHCHO + 0.01*xMECHO + 0.01*xETCHO + 0.07*RCHO + 0.08*xRCHO + 0.15*xACET + 0.09*KET2 + 0.26*xKET2 + 0.01*zR1NO3 + 0.15*zR2NO3 + 0.05*zRCNO3 + 0.12*zRHNO3 + 1.05*yROOH + 0.24*yHPCRB + 0.06*ALK3 + 0.01*ALK4 + 0.01*ALK5 + 1.31*SumRO2	1.63E-11			1.63E-11
600	Revised	ALK6_OH = 0.03*HO2 + 0.08*HPCRB	1.94E-01			1.94E-01
600	Original	ALK6_OH = 0.03*HO2 + 0.08*HPCRB	2.70E-01			2.70E-01
601	Revised	ALK6_OH + NO = NO + 0.06*xHO2 + 0.12*RO2C + 0.02*RO2XC + 0.01*xR2CO3 + 0.02*xHCHO + 0.01*xMECHO + 0.02*xRCHO + 0.04*xACET + 0.01*xKET2 + 0.01*zRCNO3 + 0.01*zRHNO3 + 0.06*yROOH + 0.04*yHPCRB + 0.14*SumRO2 + 0.01*SumRCO3	2.55E-12	-380		9.13E-12
601	Original	ALK6_OH + NO = NO + 0.06*xHO2 + 0.12*RO2C + 0.02*RO2XC + 0.01*xR2CO3 + 0.02*xHCHO + 0.01*xMECHO + 0.02*xRCHO + 0.04*xACET + 0.01*xKET2 + 0.01*zRCNO3 + 0.01*zRHNO3 + 0.06*yROOH + 0.04*yHPCRB + 0.04*ALK2 + 0.01*ALK5 + 0.14*SumRO2	2.55E-12	-380		9.13E-12

[a] k_{298} is the rate constant at 298 K and 1 atmosphere.

2.1.3 SOA production from VCPs and large alkanes

Some VCP species are precursors for SOA formation, and this chemistry has been added to SAPRC-22-VCP following the same approach as other SOA precursors. In CMAQ, OH-oxidation of precursors produces RO_2 radical species, which react with NO and HO_2 to form anthropogenic semi-volatile gases (SVAVB1, SVAVB2, SVAVB3, SVAVB4). The semi-volatile gases partition into the aerosol phase to produce SOA. Two new RO_2 species (ETHRRO2 and SILXRO2) are included in the mechanism to represent SOA production from propylene glycol (PRGLYCL), lumped large ethers (ETHR), and lumped siloxanes (SXD5). VCP alcohols included in the lumped alcohol species (ROH) do not significantly contribute to SOA production (Seltzer et al., 2021). Although some VCP species that contain an alcohol functional group, such as benzyl alcohol and several glycol ethers, do produce SOA (Sasidharan et al., 2023; Li et al., 2018), these species are represented in the model by aromatic species and ETHR, not by ROH.

Large alkanes can also produce SOA and this is represented in CMAQ using model species SOAALK. SOAALK can be included as an emitted species but is not directly associated with the alkane chemistry in the SAPRC-22 mechanism. Since reactions and definitions of large alkanes were updated to remove VCP contributions, we also introduced processes to better represent SOA production from large alkanes. We added production of an RO2 radical species (ALK6RO2) to the OH-oxidation reactions of ALK5 and ALK6 (Table 2-4), which can produce semi-volatile gases through subsequent reactions with NO and HO_2 (Table 2-5). ALK5 and ALK6 now follow similar SOA production pathways as other precursors.

The molar yields for the semi-volatile products from the new VCP and alkane related RO_2 species are based on volatility basis set (VBS) mass yield data reported in literature, as shown in Table 2-6.

2.2 Other SOA Updates

2.2.1 SOA production from IVOC and aromatics

Oxidation of intermediate volatility organic compounds (IVOC) and aromatics can lead to SOA formation. We added IVOC chemistry and updated aromatic reactions in SAPRC-22 and SAPRC-22-VCP to better represent SOA production from these species. Reaction updates are shown in Table 2-7 and include OH-oxidation of the precursor to form an RO_2 radical species, followed by RO_2 reaction with NO and HO_2 to form anthropogenic semi-volatile gases. The oxidation reactions for ethyl benzene (C2BEN) and alkylbenzenes (ARO1 and ARO2) were already included in SAPRC-22 but the RO_2 radical product has been updated to allow for SOA production. C2BEN produces the existing TOLRO2 species and a new RO_2 radical species, ARORO2, is introduced in ARO1 and ARO2 reactions. IVOC chemistry was excluded from the original version of SAPRC-22. New model species introduced by this update are provided in Table 2-8. The molar yields for the semi-volatile products of the RO_2 reactions are based on VBS mass yield data reported in literature, as shown in Table 2-8.

Table 2-5. Reactions added to SAPRC-22 to better represent SOA production from VCPs and large alkanes.

Reaction label	Reaction	A (cm^{-3} $molec^{-1}$ s^{-1})	E_a (K)	n	k_{298} (cm^{-3} $molec^{-1}$ s^{-1})[a]
AE63	ALK6RO2 + NO = NO + 0.009*SVAVB1 + 0.050*SVAVB2 + 0.140*SVAVB3 + 0.595*SVAVB4	2.55E−12	-380		9.13E−12
AE64	ALK6RO2 + HO2 = HO2 + 0.009*SVAVB1 + 0.050*SVAVB2 + 0.140*SVAVB3 + 0.595*SVAVB4	1.49E−11			1.49E−11
AE65	ETHRRO2 + NO = NO + 0.053*SVAVB1 + 0.004*SVAVB2 + 0.060*SVAVB3 + 0.152*SVAVB4	2.55E−12	-380		9.13E−12
AE66	ETHRRO2 + HO2 = HO2 + 0.053*SVAVB1 + 0.004*SVAVB2 + 0.060*SVAVB3 + 0.152*SVAVB4	1.49E−11			1.49E−11
AE67	SILXRO2 + NO = NO + 0.262*SVAVB2 + 0.446*SVAVB4	2.55E−12	-380		9.13E−12
AE68	SILXRO2 + HO2 = HO2 + 0.262*SVAVB2 + 0.446*SVAVB4	1.49E−11			1.49E−11

[a] k_{298} is the rate constant at 298 K and 1 atmosphere.

Table 2-6. New RO_2 species added to SAPRC-22 to represent SOA production from VCPs and large alkanes.

SAPRC-22-VCP Species Name	Molecular weight (g/mol)	Reference for SVAB yields
ALK6RO2	200.20	IVOCP6-ALK yields from Lu et al. (2020)
ETHRRO2	133.40	Average of yields for 5 ethers from Sasidharan et al. (2023)
SILXRO2	370.80	SILOX from Pennington et al. (2021)

Table 2-7. Reactions updated or added to SAPRC-22 to better represent SOA production from IVOC and aromatics.

Reaction label	Reaction	A (cm^{-3} $molec^{-1}$ s^{-1})	E_a (K)	n	k_{298} (cm^{-3} $molec^{-1}$ s^{-1})[a]
EBOH	C2BEN + OH = 0.36*HO2 + 0.51*xHO2 + 0.54*RO2C + 0.12*RO2XC + 0.01*xMEO2 + 0.02*xHCHO + 0.01*OLEA1 + 0.18*OLEA2 + 0.18*xGLY + 0.18*xMGLY + 0.18*xBUDAL + 0.02*xAFG1 + 0.16*xAFG2A + 0.03*xBALD + 0.16*XYNL + 0.05*zR2NO3 + 0.07*zRANO3 + 0.23*yROOH + 0.44*yRAOOH + 0.13*xBENX + 0.66*SumRO2 + TOLRO2	7.00E-12			7.00E-12
B1OH	ARO1 + OH = 0.27*HO2 + 0.48*xHO2 + 0.75*RO2C + 0.21*RO2XC + 0.05*xETO2 + 0.01*xHCHO + 0.06*xMECHO + 0.11*xETCHO + 0.01*xRCHO + 0.01*OLEA1 + 0.13*OLEA2 + 0.13*xGLY + 0.13*xMGLY + 0.13*xBUDAL + 0.01*xAFG1 + 0.12*xAFG2A + 0.2*xBALD + 0.12*XYNL + 0.03*zR1NO3 + 0.11*zR2NO3 + 0.01*zRHNO3 + 0.06*zRANO3 + 0.64*yROOH + 0.32*yRAOOH + 0.04*ARO1 + 3.11*NROG + 0.96*SumRO2 + ARORO2	7.69E-12			7.69E-12
B2OH	ARO2 + OH = ARO2_OH + 0.29*HO2 + 0.56*xHO2 + 0.6*RO2C + 0.14*RO2XC + 0.03*OLEA1 + 0.13*OLEA2 + 0.07*xGLY + 0.39*xMGLY + 0.03*xBACL + 0.03*xBUDAL + 0.07*xAFG1 + 0.3*xAFG2A + 0.04*xAFG2B + 0.04*BALD + 0.03*xBALD + 0.01*xKET2 + 0.01*LVKS + 0.04*xAFG3 + 0.08*XYNL + 0.02*zR2NO3 + 0.01*zRCNO3 + 0.11*zRANO3 + 0.1*yROOH + 0.59*yRAOOH + 0.04*yHPCRB + 0.03*xBENX + 1.38*NROG + 0.74*SumRO2 + ARORO2	2.13E-11			2.13E-11
IVOC1	IVOC + OH = IVOCRO2	4.70E−11			4.70E−11
AE59	ARORO2 + NO = NO + 0.014*SVAVB1 + 0.078*SVAVB2 + 0.190*SVAVB3 + 0.004*SVAVB4	2.55E−12	-380		9.13E−12
AE60	ARORO2 + HO2 = HO2 + 0.018*SVAVB1 + 0.101*SVAVB2 + 0.246*SVAVB3 + 0.005*SVAVB4	1.49E−11			1.49E−11
AE61	IVOCRO2 + NO = NO + 0.095*SVAVB1 + 0.044*SVAVB2 + 0.414*SVAVB3 + 0.522*SVAVB4	2.55E−12	-380		9.13E−12
AE62	IVOCRO2 + HO2 = HO2 + 0.095*SVAVB1 + 0.044*SVAVB2 + 0.414*SVAVB3 + 0.522*SVAVB4	1.49E−11			1.49E−11

[a] k_{298} is the rate constant at 298 K and 1 atmosphere.

Table 2-8. New species added to SAPRC-22 to better represent SOA production from IVOC and aromatics.

SAPRC-22 Species Name	Molecular weight (g/mol)	Reference for SVAB yields
ARORO2	127.60	IVOCP6-ARO yields from Lu et al. (2020)
IVOCRO2	193.50	Average of IVOCP5-ARO and IVOCP5-ALK yields from Lu et al. (2020)
IVOC	193.50	N/A

2.2.2 SOA production from BVOCs

The AERO7 aerosol module includes formation of SOA from acid-catalyzed uptake of isoprene epoxydiols (IEPOX) and heterogeneous uptake and hydrolysis of terpene-specific organic nitrates (MTNO3). While the U.S. EPA's CMAQ model has implemented AERO7 with the CB6 gas-phase chemistry mechanisms, AERO7 implementation with the SAPRC07 mechanisms is currently limited only to SAPRC07TIC, which is referred to as AERO7I. The AERO7I implementation of SAPRC07TIC has extensive modifications to gas-phase reactions of isoprene (ISOP) and lumped terpenes (TERP) other than α-pinene to interface with CMAQ SOA schemes. Modifications for ISOP add production of hydroxymethyl-methyl-α-lactone (HMML) and methacrylic acid epoxide (MAE) that can then form SOA via heterogeneous uptake to aerosols (note that the AERO6 implementation has a more condensed treatment of IEPOX and SOA formation without HMML or MAE formation).

These SOA formation pathways from isoprene and terpenes are not included in the public domain version of CMAQ with the SAPRC-22 gas-phase chemistry mechanism, because of the limited scope of the EPA-funded SAPRC-22 chemistry implementation project. Making the needed changes to SAPRC-22 would have created a new mechanism and updating SAPRC-22 ISOP chemistry to produce IEPOX (even for the simple treatment in AERO6), HMML and MAE would have substantially altered the mechanism and could have changed oxidant production in ways that would need to be evaluated. Similarly, Ramboll did not update the terpene chemistry to produce MTNO3 in the EPA project because the SAPRC07 updates to TERP and α-pinene (APIN) differed for reasons that weren't fully apparent at the time. Instead, the SAPRC-22 implementation for EPA utilizes the CMAQ AERO6 SOA schemes for ISOP (not including IEPOX), TERP and APIN. Specifically, ISOP oxidation reactions produce species ISOPRXN that then links to SOA production, and TERP/APIN oxidation reactions produce species TERPRXN, except for the APIN reaction with NO_3 that doesn't produce TERPRXN (consistent with AERO7). SAPRC-22 adds β-pinene (BPINE) as an explicit species and SOA formation from BPINE is represented in the same way as TERP by adding TERPRXN as a product of the reactions of BPINE with OH, O_3, NO_3 and $O(^3P)$.

The Air District believed that these SOA formation pathways from IEPOX and MTNO3, which were not included in the base SAPRC-22 mechanism, were important and requested Ramboll to update the SAPRC-22 chemistry to include these pathways. Although this task was not in the original scope of work for the CRC/Air District project, Ramboll agreed to make the requested updates. The updated aerosol module is referred to as AERO6.8.

IEPOX is a product of the reactions of OH with unsaturated OH-substituted hydroperoxides formed when peroxy radicals formed in the reactions of VOCs with OH react with HO_2. All these unsaturated hydroperoxides are lumped into the model species "RUOOH", and the reaction of OH with the set of compounds making up this model species (dominated by isoprene products) produce IEPOX with a yield of 59%.

After discussions with the SAPRC-22 mechanism developer, Dr. Bill Carter, Ramboll updated the SAPRC-22 chemistry mechanism as follows:

1. Introduced new species (RIOOH, RIOOH_OH, yRIOOH) and reactions of these species as analogues of existing species (RUOOH, RUOOH_OH, yRUOOH) and existing reactions to replicate the existing RUOOH scheme. These species and reactions were added to keep the RIOOH chemistry specific to isoprene, and the rate constants for the new reactions were identical to the rate constants for the existing RUOOH scheme.

2. Modified existing isoprene reactions that form yRUOOH in the original mechanism to form yRIOOH instead.

3. Created a new model species (IEPOX) and added the reaction of RIOOH with OH to form IEPOX with a 59% yield. This new reaction has the same rate constant as the existing reaction of RUOOH with OH to produce the lumped alkane, ALK5, with a 59% yield.

4. Added a new reaction of IEPOX with OH, using rate constant data generated by MechGen.

5. Added reactions and species (IEPOXP, AIETETJ, AIEOSJ, ADIMJ) to represent SOA formation via heterogeneous uptake of IEPOX to aerosols. These reactions and species are identical to those in the AERO7I version of SAPRC07TIC.

The updates for SOA formation from terpene nitrates were more substantial than the IEPOX updates because it involved modifications to the existing reactions of 4 biogenic species: α-pinene (APINE), β-pinene (BPINE), sesquiterpenes (SESQ), and other terpenes (TERP) with the NO_3 radical and the addition of several new species and reactions (8 organic terpene nitrate species and 28 reactions) to represent the subsequent chemistry of the new organic nitrate products of the 4 reactions. We also simplified autooxidation by assuming that the reaction with NO of autooxidation species formed in the TERP + NO3 and SESQ + NO3 reactions was negligible and by folding the products of the fast unimolecular reactions of the autooxidation species into the original parent reactions.

Table 2-9 lists the new species added to represent the organic nitrate species formed from reactions of terpenes with the NO3 radical. The left column shows the existing organic nitrate products from the reactions of all alkenes (including anthropogenic alkenes, isoprene, and terpenes) with the NO_3 radical, while the right column shows the new species added for the terpene + NO_3 reactions. The new species TCNO3, TPNO3, TDNO3 and T1NO3 are terpene nitrates that can hydrolyze in aerosol according to the CMAQ AERO7 scheme.

Table 2-10 shows the revised existing reactions of APINE, BPINE, SESQ and TERP with the NO_3 radical. The revisions are highlighted. The changes are only to the organic nitrate products of these reactions. As discussed above, for reactions SQN3 and TPN3, the autooxidation products (SESQ_N3 and TERP_N3, respectively) are replaced by the products of their fast unimolecular reactions. Table 2-11 shows the new reactions added to the modified SAPRC-22 chemistry mechanism.

Table 2-9. New organic nitrate species from terpene precursors in modified SAPRC-22.

Nitrate species from NO3 + alkenes in SAPRC-22	Nitrate species from NO3 + terpenes in modified SAPRC-22
Volatile organic carbonyl nitrates	
RCNO3	TCNO3
xRCNO3	xTCNO3
zRCNO3	zTCNO3
Organic nitrates with hydroperoxy groups	
RPNO3	TPNO3
yRPNO3	yTPNO3
Volatile organic dinitrates	
RDNO3	TDNO3
zRDNO3	zTDNO3
Other volatile organic nitrates that react slowly with OH radicals	
R1NO3	T1NO3

Table 2-10. Terpene reactions with NO_3 radicals in the modified SAPRC-22 mechanism.

Reaction label	Reaction	Reaction Rate
APN3	APINE + NO3 = 0.81*xNO2 + 0.81*RO2C + 0.19*RO2XC + 0.81*xRCHO + yTPNO3 + 0.19*zTCNO3 + SumRO2	Same as existing SAPRC-22 reaction
BPN3	BPINE + NO3 = 0.02*OH + 0.04*xOH + 0.18*xHO2 + 2.25*RO2C + 0.63*RO2XC + 0.14*xR2CO3 + 0.04*xHCHO + 0.02*xRCHO + 0.27*xACET + 0.14*xPACID + 0.02*TCNO3 + 0.22*xTCNO3 + 0.43*zTCNO3 + yTPNO3 + 0.19*zTDNO3 + 0.04*CO2 + 2.88*SumRO2 + TRPRXN	Same as existing SAPRC-22 reaction
SQN3[1]	SESQ + NO3 = 0.74*xNO2 + 0.03*OH + 0.01*HO2 + 0.82*RO2C + 0.22*RO2XC + 0.74*xOLEA2 + 0.03*TCNO3 + 0.01*zTCNO3 + yTPNO3 + 0.21*zTDNO3 + 1.04*SumRO2 + SESQRXN	Same as existing SAPRC-22 reaction
TPN3[2]	TERP + NO3 = 0.51*xNO2 + 0.11*OH + 0.01*xOH + 0.04*HO2 + 0.05*xHO2 + 1.12*RO2C + 0.28*RO2XC + 0.01*xHCHO + 0.29*xRCHO + 0.21*xOLEA2 + 0.15*xACET + 0.01*xMVK + 0.01*xOLEP + 0.11*TCNO3 + 0.07*xTCNO3 + 0.08*zTCNO3 + yTPNO3 + 0.19*zTDNO3 + 0.04*yROOH + 0.01*yRUOOH + 1.4*SumRO2 + TRPRXN	Same as existing SAPRC-22 reaction

[1]Autooxidation product SESQ_N3 is replaced by the products of its unimolecular reaction
[2]Autooxidation product TERP_N3 is replaced by the products of its unimolecular reaction

Table 2-11. New reactions added to SAPRC-22 to represent terpene organic nitrate chemistry.

Reaction label	Reaction	Reaction Rate
T310	xTCNO3 + NO = NO + TCNO3	Same as xRCNO3 + NO reaction
T311	xTCNO3 + HO2 = HO2	Same as xRCNO3 + HO2 reaction
T312	xTCNO3 + NO3 = NO3 + TCNO3	Same as xRCNO3 + NO3 reaction
T313	xTCNO3 + SumRO2 = SumRO2 + 0.5*TCNO3	Same as xRCNO3 + SumRO2 reaction
T314	xTCNO3 + SumRCO3 = SumRCO3 + TCNO3	Same as xRCNO3 + SumRCO3 reaction
T420	yTPNO3 + NO = NO	Same as yRPNO3 + NO reaction
T421	yTPNO3 + HO2 = HO2 + TPNO3	Same as yRPNO3 + HO2 reaction
T422	yTPNO3 + NO3 = NO3	Same as yRPNO3 + NO3 reaction
T423	yTPNO3 + SumRO2 = SumRO2 + 0.5*T1NO3	Same as yRPNO3 + SumRO2 reaction
T424	yTPNO3 + SumRCO3 = SumRCO3	Same as yRPNO3 + SumRCO3 reaction
T440	zTCNO3 + NO = NO + TCNO3	Same as zRCNO3 + NO reaction
T441	zTCNO3 + HO2 = HO2	Same as zRCNO3 + HO2 reaction
T442	zTCNO3 + NO3 = NO3 + KET2 + HO2	Same as zRCNO3 + NO3 reaction
T443	zTCNO3 + SumRO2 = SumRO2 + 0.5*KET2 + 0.5*HO2	Same as zRCNO3 + SumRO2 reaction
T444	zTCNO3 + SumRCO3 = SumRCO3 + KET2 + HO2	Same as zRCNO3 + SumRCO3 reaction
T455	zTDNO3 + NO = NO + TDNO3	Same as zRDNO3 + NO reaction
T456	zTDNO3 + HO2 = HO2	Same as zRDNO3 + HO2 reaction
T457	zTDNO3 + NO3 = NO3 + T1NO3 + HO2	Same as zRDNO3 + NO3 reaction
T458	zTDNO3 + SumRO2 = SumRO2 + 0.5*T1NO3 + 0.5*HO2	Same as zRDNO3 + SumRO2 reaction
T459	zTDNO3 + SumRCO3 = SumRCO3 + T1NO3 + HO2	Same as zRDNO3 + SumRCO3 reaction
TN4OH	TCNO3 + OH = 0.34*NO2 + 0.1*xNO2 + 0.02*OH + 0.01*xOH + 0.1*HO2 + 0.13*xHO2 + 0.49*RO2C + 0.07*RO2XC + 0.05*xMECO3 + 0.07*R2CO3 + 0.08*xR2CO3 + 0.03*MACO3 + 0.13*xHCHO + 0.05*xMECHO + 0.05*RCHO + 0.05*xRCHO + 0.01*xGLY + 0.05*MGLY + 0.02*xACET + 0.12*KET2 + 0.01*xKET2 + 0.01*PACID + 0.05*xPACID + 0.04*OLEP + 0.12*TCNO3 + 0.21*xTCNO3 + 0.07*zTCNO3 + 0.03*yTPNO3 + 0.03*yHPCRB + 0.06*ALK2 + 4.74*NROG + 0.01*CO2 + 0.01*CO + 0.56*SumRO2 + 0.09*SumRCO3	Same as RCNO3 + OH reaction
TN4HV	TCNO3 = 0.77*NO2 + 0.04*xNO2 + 0.01*xOH + 0.63*HO2 + 0.19*xHO2 + 0.53*RO2C + 0.1*RO2XC + 0.07*ETO2 + 0.11*MECO3 + 0.04*R2CO3 + 0.03*xR2CO3 + 0.11*HCHO + 0.02*xHCHO + 0.05*MECHO + 0.02*RCHO + 0.07*xRCHO + 0.09*OLEA2 + 0.03*MACR + 0.04*AFG2A + 0.07*xACET + 0.04*xKET2 + 0.04*OACID + 0.03*xOACID + 0.08*PACID + 0.06*xPACID + 0.06*TCNO3 + 0.02*xTCNO3 + 0.08*zTCNO3 + 0.03*xRHNO3 + 0.02*TPNO3 + 0.17*yTPNO3 + 0.02*zRDNO3 + 0.1*HPCRB + 0.22*yHPCRB + 8.77*NROG + 0.01*CO2 + 0.34*CO + 0.71*SumRO2 + 0.14*SumRCO3	Same as RCNO3 photolysis reaction

Reaction label	Reaction	Reaction Rate
TNDOH	TDNO3 + OH = 0.53*NO2 + 0.04*xNO2 + 0.01*HO2 + 0.25*xHO2 + 0.6*RO2C + 0.15*RO2XC + 0.2*xHCHO + 0.03*xACET + 0.1*xKET2 + 0.02*TCNO3 + 0.25*xTCNO3 + 0.01*zTCNO3 + 0.52*RHNO3 + 0.05*xTDNO3 + 0.13*zTDNO3 + 0.01*CO + 0.75*SumRO2	Same as RDNO3 + OH reaction
TNDHV	TDNO3 = 1.90*NO2 + 0.05*HO2 + 0.01*xHO2 + 0.08*RO2C + 0.03*RO2XC + 0.01*xR2CO3 + 0.3*HCHO + 0.21*OLEA1 + 0.35*OLEA2 + 0.02*xACET + 0.05*KET2 + 0.25*MVK + 0.02*TPNO3 + 0.03*TCNO3 + 0.01*xTCNO3 + 0.03*zTCNO3 + 0.04*HPCRB + 0.11*SumRO2	Same as RDNO3 photolysis reaction
TN6OH	TPNO3 + OH = 0.01*zRNNO3 + 0.40*NO2 + 0.07*xNO2 + 0.24*OH + 0.14*HO2 + 0.11*xHO2 + 0.23*RO2C + 0.05*RO2XC + 0.1*xHCHO + 0.04*xOLEA1 + 0.01*xOLEA2 + 0.03*xKET2 + 0.02*xMVK + 0.08*TCNO3 + 0.1*xTCNO3 + 0.16*RHNO3 + 0.13*TPNO3 + 0.01*xTPNO3 + 0.14*yTPNO3 + 0.03*zRDNO3 + 0.32*ROOH + 0.08*HPCRB + 0.01*xHPCRB + 0.28*SumRO2	Same as RPNO3 + OH reaction
TN6HV	TPNO3 = 0.84*NO2 + OH + 0.15*HO2 + 0.01*RO2C + 0.63*HCHO + 0.43*OLEA1 + 0.1*OLEA2 + 0.12*MVK + 0.15*OLEP + 0.01*TPNO3 + 0.14*TCNO3 + 0.01*yTPNO3 + 0.03*HPCRB + 0.01*SumRO2	Same as RPNO3 photolysis reaction
TN1OH	T1NO3 + OH = 0.17*NO2 + 0.41*xNO2 + 0.01*HO2 + 0.29*xHO2 + 0.99*RO2C + 0.12*RO2XC + 0.1*xHCHO + 0.29*xMECHO + 0.05*xETCHO + 0.02*xRCHO + 0.05*ACET + 0.25*xACET + 0.05*MEK + 0.04*xMEK + 0.07*KET2 + 0.05*xKET2 + 0.19*xTCNO3 + 0.1*xRHNO3 + 0.01*TPNO3 + 1.12*yTPNO3 + 0.12*zTDNO3 + 1.12*SumRO2	Same as R1NO3 + OH reaction
TN1HV	T1NO3 = NO2 + 0.19*HO2 + 0.38*xHO2 + 0.45*RO2C + 0.06*RO2XC + 0.32*ETO2 + 0.04*TBUO + 0.01*xTBUO + 0.05*xHCHO + 0.12*MECHO + 0.03*ETCHO + 0.03*xETCHO + 0.02*xRCHO + 0.34*ACET + 0.12*xACET + 0.11*MEK + 0.05*KET2 + 0.22*xKET2 + 0.01*zR1NO3 + 0.06*zRHNO3 + 0.51*yROOH + 0.83*SumRO	Same as R1NO3 photolysis reaction

3.0 BASE CASE MODELING

The Air District conducted three base case simulations with different combinations of chemical mechanism and biogenic VOC emissions. Table 3-1 lists the combinations used in the simulations.

Table 3-1. Base case CMAQ simulations.

Model scenario	Chemistry	Biogenic Emissions[a]	Aerosol Module
1	SAPRC-22 (without VCPs)	BEIS3.61	AERO6.8
2	SAPRC-22-VCP	BEIS3.61	AERO6.8
3	SAPRC-22-VCP	MEGAN 3.2	AERO6.8

[a] BEIS = Biogenic Emission Inventory System; MEGAN = Model of Emissions of Gases and Aerosols from Nature

Ramboll provided species mappings for SAPRC-22 with and without VCPs to the Air District to facilitate creation of initial and boundary conditions (ICs/BCs) as well as anthropogenic VOC emissions for the Air District's CMAQ simulations (see Section 3.2.1).

As a reference point for the simulations conducted here, the Air District also provided results from its most recent modeling platform using CMAQ with SAPRC07 chemistry, MEGAN 3.2 biogenic emissions, and the AERO7 aerosol module. Below, we describe the modeling platform that the Air District uses in their applications.

3.1 Model Setup

The Air District applied CMAQ over the entire 2022 calendar year to simulate spatial and temporal patterns of ambient $PM_{2.5}$, ozone, and precursors across the Bay Area. CMAQ was run on 2 grid domains (Figure 3-1) — a regional grid covering most of California with 4 km grid resolution, and a Bay Area grid with 1 km grid resolution.

Boundary conditions for all chemical species on the 4 km California grid were extracted from near-real time global air quality forecasts from the Whole Atmosphere Community Climate Model (WACCM)[6] available from the National Center for Atmospheric Research[7]. CMAQ was run for the 4 km California grid first, then three-dimensional output was used to extract boundary conditions for the 1 km Bay Area grid, which was run subsequently. All CMAQ simulations analyzed in this project were conducted by the Air District on the single Bay Area grid using the same boundary conditions from the single previous run on the California grid.

Hourly and spatially-varying meteorological inputs for both grids were derived by the Air District using the Weather Research and Forecasting Model (WRF)[8] to simulate weather conditions for the entire year. Raw output data from WRF were processed to CMAQ inputs using the EPA's Meteorology-Chemistry Interface Program (MCIP)[9].

[6] https://ncar.ucar.edu/what-we-offer/models/whole-atmosphere-community-climate-model-waccm
[7] https://ncar.ucar.edu/
[8] https://www.mmm.ucar.edu/models/wrf
[9] https://cfpub.epa.gov/si/si_public_record_report.cfm?Lab=NERL&dirEntryId=215883

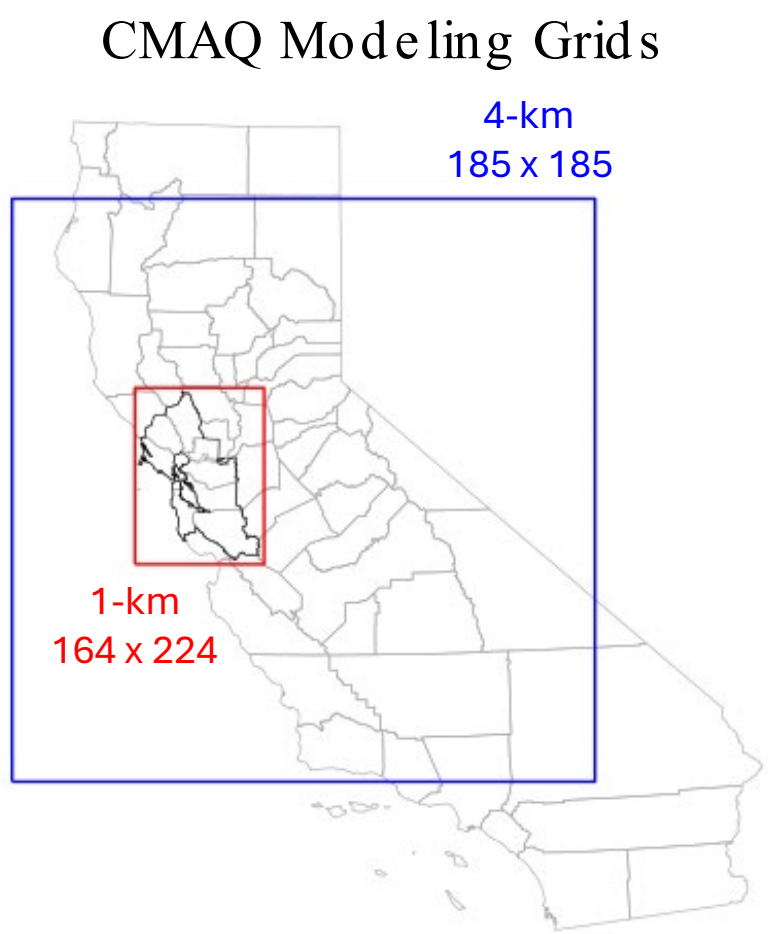

Figure 3-1. The Air District CMAQ modeling domains.

For the reference case, the Air District used the Statewide Air Pollution Research Center 2007 photochemistry mechanism that was expanded to include certain toxics (SAPRC07TC). Aerosol chemistry was simulated using the AERO7 module.

3.2 Model Emissions

For both modeling grids shown in Figure 3-1, emissions inputs to CMAQ were based on the Air District's emissions estimates for permitted sources and selected area sources. On-road mobile source emissions were based on the California Air Resources Board's (CARB) EMFAC2021 model, and offroad mobile source emissions are derived from CARB's California Emissions Projection Analysis Model (CEPAM2022v1.01) database. CMAQ ready anthropogenic emissions inputs were prepared using SMOKE 4.7. The latest CARB spatial surrogate data were used to grid emissions: SNP20221001 surrogate files; ESTA surrogates for mobile sources; and internal surrogates for residential wood combustion in Bay Area counties.

The Air District has historically used the BEIS3.61 to estimate biogenic emissions, however, the agency now uses MEGAN v3.2 with recently improved inputs for the Bay Area (Guenther et al., 2025). Sea salt emissions were estimated using an in-line sea spray algorithm within CMAQ. The 2022 emission inventory does not include wildfire emissions as there were no substantial smoke impacts in the Bay Area during 2022. All emission inputs were temporally allocated to each hour, day-of-week,

and season/month and chemically speciated for the appropriate gas phase and aerosol chemistry mechanisms.

3.2.1 Anthropogenic emissions for SAPRC-22 and SAPRC-22-VCP simulations

Ramboll developed speciation mappings for SMOKE to support the SAPRC-22 and SAPRC-22-VCP simulations. Speciation mapping refers to translating the detailed VOC compounds present in VOC speciation profiles to the VOC model species used by condensed chemical mechanisms such as SAPRC-22. We first developed mappings for VOCs in EPA's SPECIATE (version 5.3)[10] profiles to process SAPRC-22 species, following assignments from the chemical speciation database SpecDB (Carter, 2015). The SAPRC-22 mappings were then updated to include VCP model species by first mapping the explicit VCPs in SAPRC-22-VCP, mapping the lumped siloxanes to model species SXD5, and then assigning lumped oxygenates with the priority of ethers (ETHR) > alcohols (ROH) > esters (ESTR).

We ran Ramboll's Speciation Tool to create SMOKE-ready VOC speciation profiles for both SAPRC-22 and SAPRC-22-VCP, generating a total of 2,676 profiles from SPECIATE5.3. To implement SPECIATE5.3 profiles in their SMOKE modeling setup, the Air District applied a cross reference from source category ID to profile ID. The Air District ran SMOKE and provided the SMOKE reports to Ramboll for review. Ramboll used these reports to prepare emission summaries by sector for both SAPRC-22 and SAPRC-22-VCP and to estimate SOA formation potential from the two chemistry mechanisms.

Table 3-2 and Table 3-3 show the emission summaries by sector and summed over all counties in the 1 km domain for the SAPRC-22 and SAPRC-22-VCP speciation, respectively. CO and NOx emissions are identical between the two mechanisms and only VOCs vary due to differences in speciation. VCP species are primarily emitted from area sources (excluding residential wood), so emission differences are isolated to that sector and are minor (<1%).

Table 3-2. SAPRC-22 emissions (tons/day) for each sector, summed across all counties.

Species	Area (excl. Residential Wood)	On-road Mobile	Non-road mobile	Point (Air District)	Point (non-Air District)	Residential Wood Combustion	Total Emissions
CO	44.2	435.0	673.0	18.0	6.12	69.3	1,240
NOx	29.5	87.5	118.0	18.4	3.64	1.26	258
NO	16.9	50.2	67.6	10.5	2.09	0.725	148
NO2	2.95	8.75	11.8	1.84	0.364	0.126	25.8
Total VOC	538.0	54.0	71.9	37.7	30.5	19.0	752

[10] EPA's SPECIATE 5.3 Addendum

Table 3-3. SAPRC-22-VCP emissions (tons/day) for each sector, summed across all counties

Species	Area (excl. Residential Wood)	On-road Mobile	Non-road mobile	Point (Air District)	Point (non-Air District)	Residential Wood Combustion	Total Emissions
CO	44.2	435.0	673.0	18.0	6.12	69.3	1,240
NOx	29.5	87.5	118.0	18.4	3.64	1.26	258
NO	16.9	50.2	67.6	10.5	2.09	0.725	148
NO2	2.95	8.75	11.8	1.84	0.364	0.126	25.8
Total VOC	542.0	54.0	71.9	37.7	30.5	19.0	755

3.2.2 SAPRC-22 vs SAPRC-22-VCP SOA forming potential of precursors

To understand how the addition of VCPs impacts SOA formation, we calculated the emission-weighted SOA potential of each anthropogenic precursor for both the base SAPRC-22 and SAPRC-22-VCP mechanisms. SOA potential is calculated here by multiplying the emissions by the SOA yield at 10 $\mu g/m^3$ of total OA at 298K under high NO conditions. The anthropogenic SOA precursors and their SOA yields are listed in Table 3-4.

Table 3-4. Anthropogenic SOA precursors and SOA yields.

Precursor	Mechanism	SOA yield (g/g)
SOAALK	SAPRC-22	0.015
ALK5	SAPRC-22-VCP	0.075
ALK6	SAPRC-22-VCP	0.15
OXYL	Both	0.05
MXYL	Both	0.05
PXYL	Both	0.05
BZ123	Both	0.05
BZ124	Both	0.05
BZ135	Both	0.05
STYRS	Both	0.05
BENZ	Both	0.14
TOLU	Both	0.08
C2BEN	Both	0.08
ARO1	Both	0.25
ARO2	Both	0.25
NAPS	Both	0.21
IVOC	Both	0.35
ETHR	SAPRC-22-VCP	0.14
PRGLYCL	SAPRC-22-VCP	0.07
SXD5	SAPRC-22-VCP	0.16

Introducing new VCP species that form SOA (ETHR, PRGLYCL, SXD5) and updating the treatment of SOA formation from large alkanes increases the SOA potential for SAPRC-22-VCP by ~55% compared to the base mechanism (Figure 3-2). This occurs despite emissions of SOA precursors decreasing slightly in SAPRC-22-VCP due to differences in the speciation mapping (Figure 3-3). In particular, more VOCs are mapped to model species with higher SOA yields in SAPRC-22-VCP. SOAALK dominates the SOA precursor emissions in SAPRC-22 but has a small SOA yield so it only contributes 12% to the SOA potential. ALK5 and ALK6 in SAPRC-22-VCP, on the other hand, have much higher SOA yields, which significantly increases the importance of alkanes to SOA formation. The new VCP species ETHR also has a comparatively high SOA yield of 0.14 g/g and contributes 17% of the total SOA potential in SAPRC-22-VCP. Most of the emitted VOCs that are mapped to ETHR in SAPRC-22-VCP are mapped to SOAALK in SAPRC-22, which has a much lower SOA yield. SOA formation from IVOC is important for both mechanisms, even though it only contributes 6% of the total SOA precursor emissions, due to the large SOA yield of 0.35 g/g. SOA formation from IVOC was not included in the EPA version of SAPRC-22 and was added to both the SAPRC-22 and SAPRC-22-VCP mechanisms in this work.

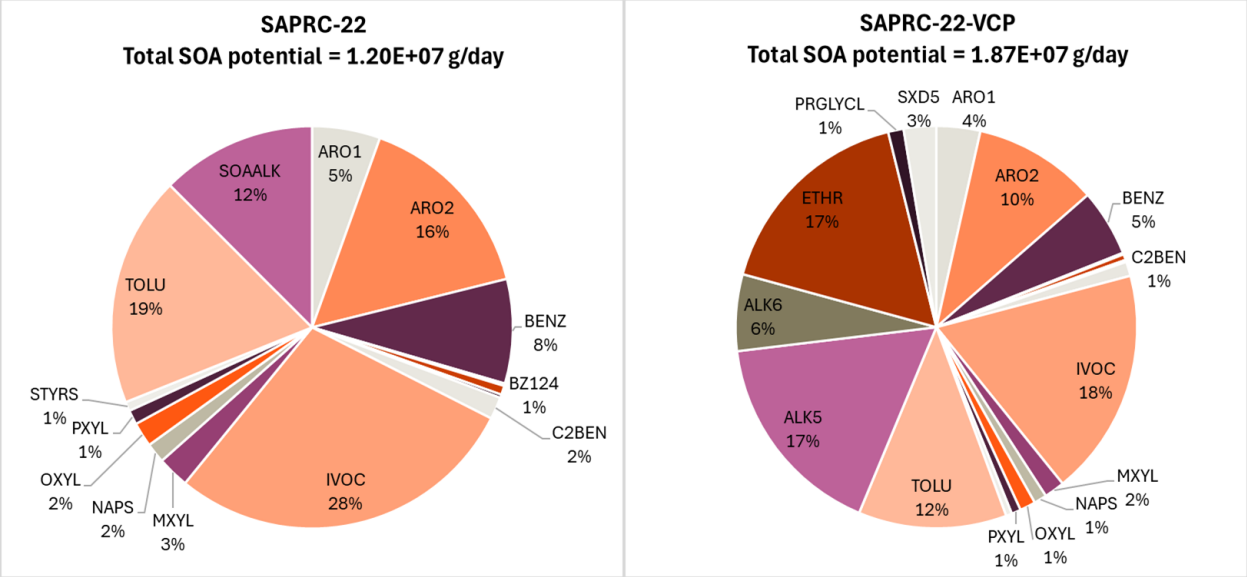

Figure 3-2. Total SOA potential and contribution of SOA precursor species for SAPRC-22 and SAPRC-22-VCP.

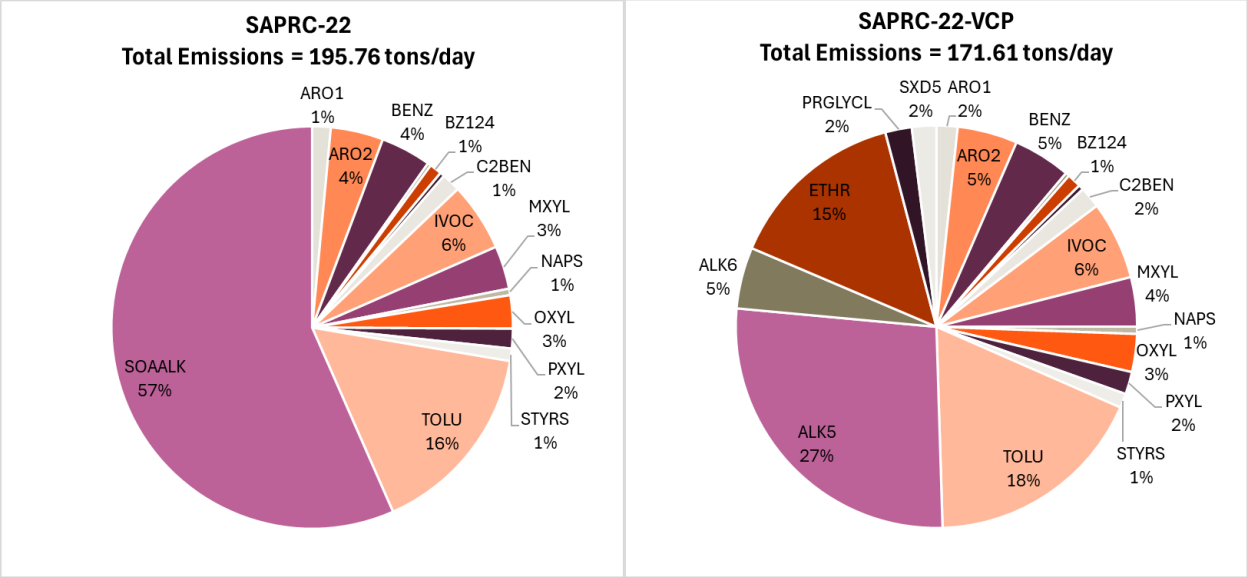

Figure 3-3. Emissions of anthropogenic SOA precursor species within the Air District's 1-km regional modeling domain for SAPRC-22 and SAPRC-22-VCP.

3.2.3 Biogenic emissions

As mentioned previously, the Air District has historically used BEIS for biogenic emissions but has now moved to the MEGAN model. However, as part of this study, the Air District conducted base case simulations with both sets of biogenic emissions. To understand the differences between the two biogenic emissions estimates, we constructed summary tables of the 5 key biogenic VOCs (isoprene, α-pinene, β-pinene, sesquiterpenes, and other terpenes) for each month of the 2022 simulation year.

Table 3-5 and Table 3-6 show the monthly and annual average total emissions (over the Bay Area domain) in metric tons per day for the 5 biogenic species from BEIS and MEGAN, respectively. Total emissions from MEGAN are lower than BEIS for isoprene, α-pinene, β-pinene, and sesquiterpenes, but higher than BEIS for other terpenes. A comparison with the anthropogenic VOC emissions in Table 3-2 shows that total BVOC emissions from BEIS are about 18% of the total VOC emissions in the domain. For MEGAN, the total BVOC emissions are about 12% of the total VOC emissions.

BVOC emission estimates from the two models have been compared in several studies. The most recent studies that compared MEGAN 3.2 (the version used in this study) with BEIS 3.6 include Wei et al. (2024) and Gao et al. (2025). Differences between BEIS and MEGAN can be attributed to both differences in input data and model formulation. MEGAN uses updated satellite-derived vegetation datasets, species-specific emission factors, canopy-scale process algorithms, and detailed representations of leaf area and plant functional types, whereas BEIS employs a more simplified representation of vegetation and emission processes. For example, MEGAN estimates standard conditions using a canopy-scale emission factor, whereas BEIS relies on a leaf-scale factor (Hogrefe et al., 2011). BEIS adjusts for temperature and light only at the top of the canopy, while MEGAN uses a parameterized canopy environment emission model to calculate temperature and light adjustments within and throughout the entire canopy (Hogrefe et al., 2011). MEGAN can represent sunlit and shaded leaves, leaf age, soil moisture, CO_2 or ozone-related adjustments depending on version/configuration, plus optional drought, high/low temperature and wind stress in MEGAN 3.2 (Gao et al., 2025; Guenther et al., 2025).

The version of MEGAN 3.2 used in this study was designed to improve BVOC emission estimates for urban areas within the Air District jurisdiction by refining landcover, leaf area index (LAI) inputs, growth form, and species-specific emission factors, especially for urban trees (Guenther et al., 2025). The LAI inputs were updated using high-resolution (300-m, 10-day) ESA satellite data, validated with field measurements at urban sites. This replaced older, less accurate interpolation-derived LAI data.

Figures 3-4 through Figure 3-8 show the spatial differences between total monthly MEGAN and BEIS emissions for the 5 biogenic species for a summer month (July). As can be seen from these plots, there are large spatial differences between the biogenic VOC emission estimates from the two models. In general, MEGAN estimates more α-pinene emissions (Figure 3-4) in some populated areas (e.g., portions of Alameda County, Santa Clara County, Contra Costa County) than BEIS, while the opposite is true for less populated and rural areas. However, the magnitudes of the MEGAN decreases are larger than the magnitudes of the MEGAN increases. The differences between the 2 biogenic emissions models for β-pinene (Figure 3-5) are qualitatively similar to those for α-pinene, but there are less areas with increases. For isoprene (Figure 3-6), MEGAN predicts higher emissions than BEIS in agricultural areas (e.g., San Joaquin County) as well as in San Mateo, Santa Cruz and Marin Counties, but lower emissions in Alameda and Santa Clara County. The differences for sesqiterpenes (Figure 3-7) are qualitatively similar to those for β-pinene. There are widespread and large increases in MEGAN estimates compared to BEIS estimates for other terpenes (Figure 3-8), with small decreases in a few areas.

Table 3-5. BEIS estimates of monthly and annual average biogenic species emissions (tons/day) over the 1 km modeling domain.

	APINE	BPINE	ISOP	SESQ	TERP
January	10.3	5.6	16.5	1.9	7.2
February	11.9	6.5	33.45	2.7	8.3
March	12.8	7.1	56.3	2.9	8.9
April	14.2	8.0	88.8	3.9	10.0
May	20.1	11.30	166.9	7.4	13.8
June	28.4	16.1	269.9	13.6	19.5
July	29.4	16.7	262.9	13.4	19.9
August	31.6	17.9	257.8	15.2	21.4
September	31.1	17.5	187.5	17.4	21.3
October	20.4	11.4	80.8	6.8	14.0
November	10.0	5.5	16.0	1.8	7.1
December	8.0	4.3	6.5	1.2	5.7
Annual	19.1	10.7	120.8	7.4	13.1

Table 3-6. MEGAN estimates of monthly and annual average biogenic species emissions (tons/day) over the 1 km modeling domain.

	APINE	BPINE	ISOP	SESQ	TERP
January	2.4	1.3	11.8	1.1	21.5
February	3.8	1.7	20.4	1.8	28.0
March	5.0	2.1	27.9	2.3	32.8
April	6.6	2.4	37.8	2.9	36.9
May	11.5	3.5	69.8	5.4	50.4
June	17.8	4.8	110.6	8.8	67.3
July	15.4	4.1	99.0	8.0	58.8
August	16.2	4.3	102.9	8.5	60.7
September	15.5	3.9	97.4	8.3	54.0
October	6.2	2.0	38.8	3.1	29.5
November	1.6	0.7	8.6	0.7	12.0
December	1.0	0.6	4.5	0.5	10.5
Annual	8.6	2.6	52.6	4.3	38.6

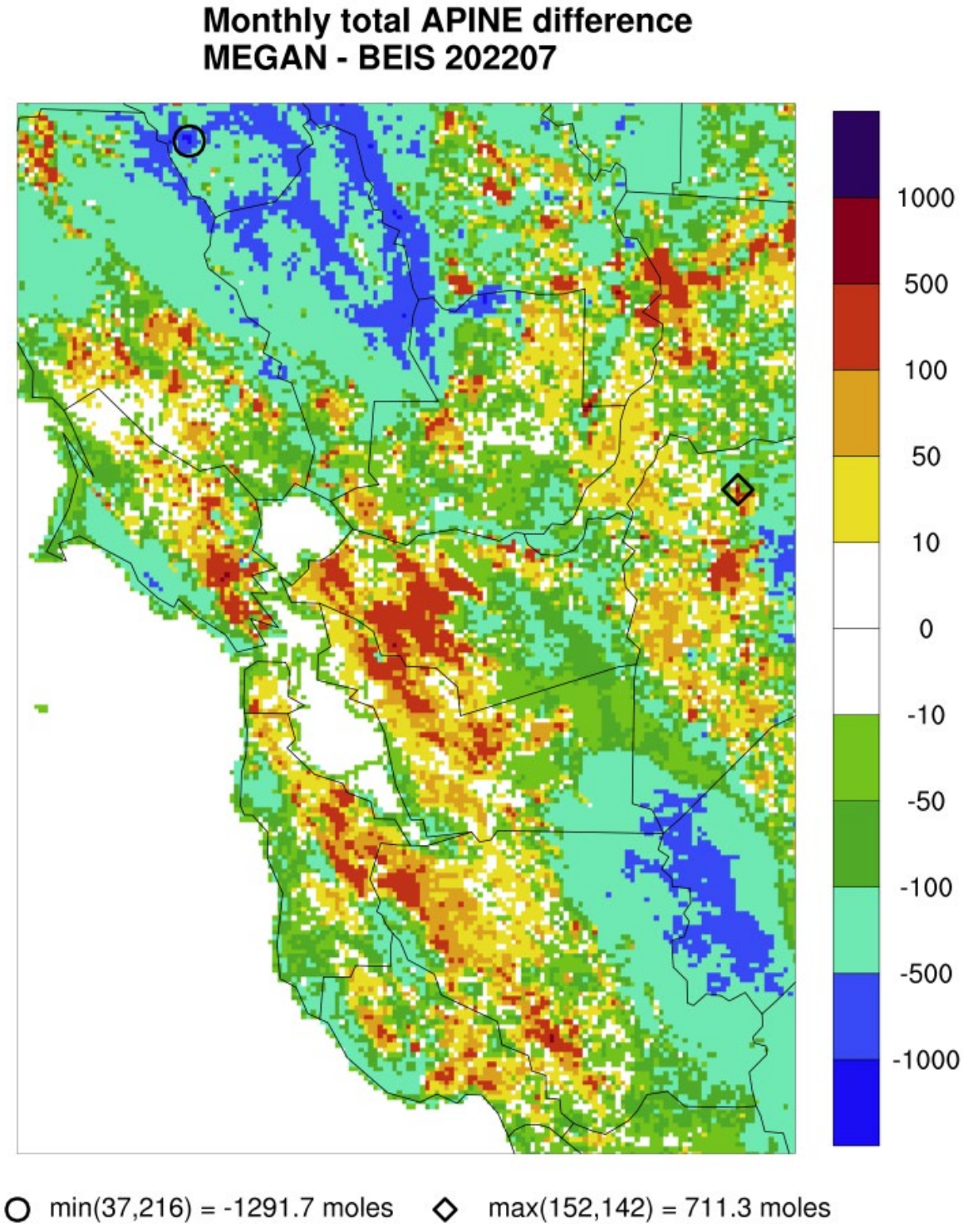

Figure 3-4. Differences between total MEGAN and BEIS emissions (in moles) of α-pinene in July 2022.

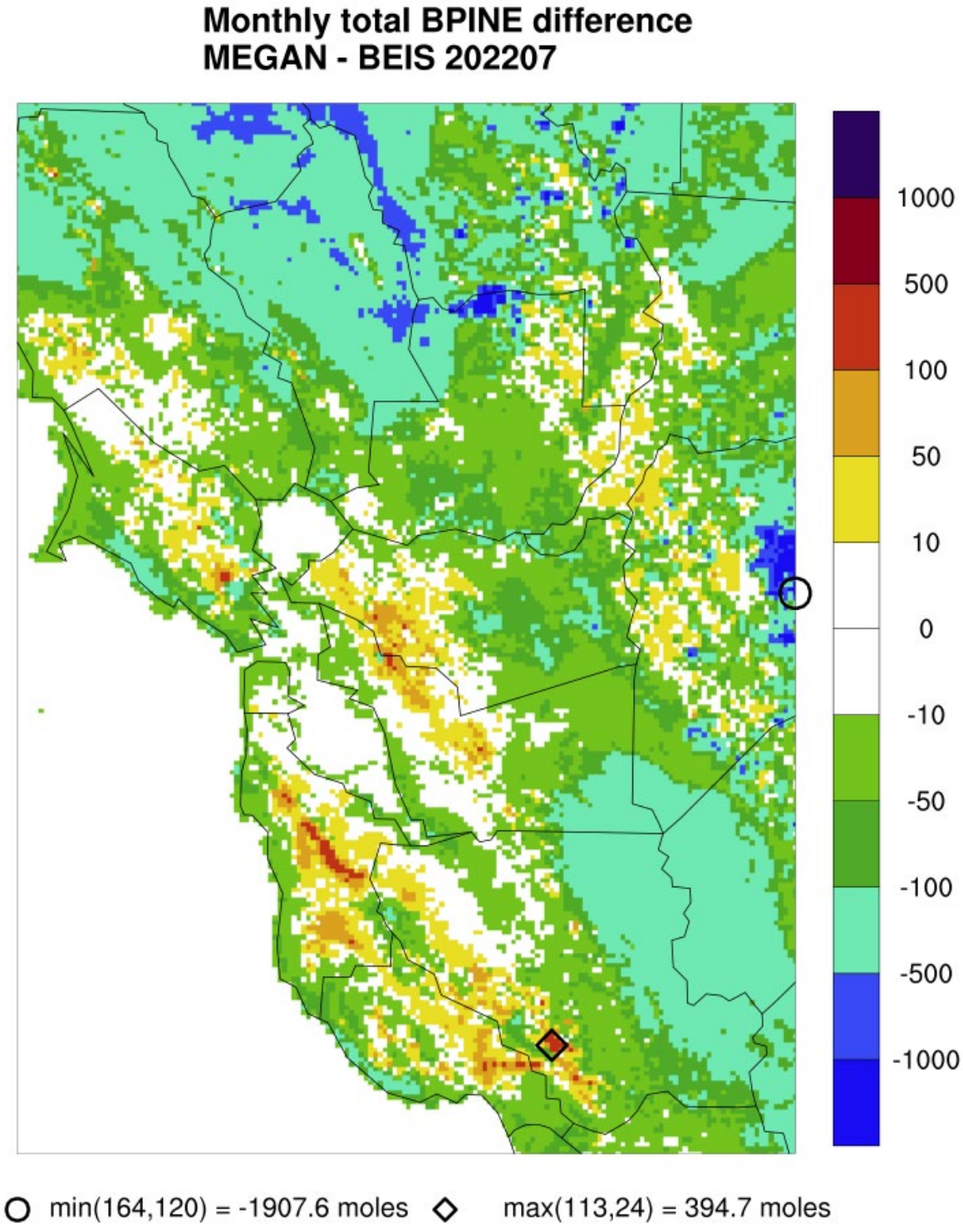

Figure 3-5. Differences between total MEGAN and BEIS emissions (in moles) of β-pinene in July 2022.

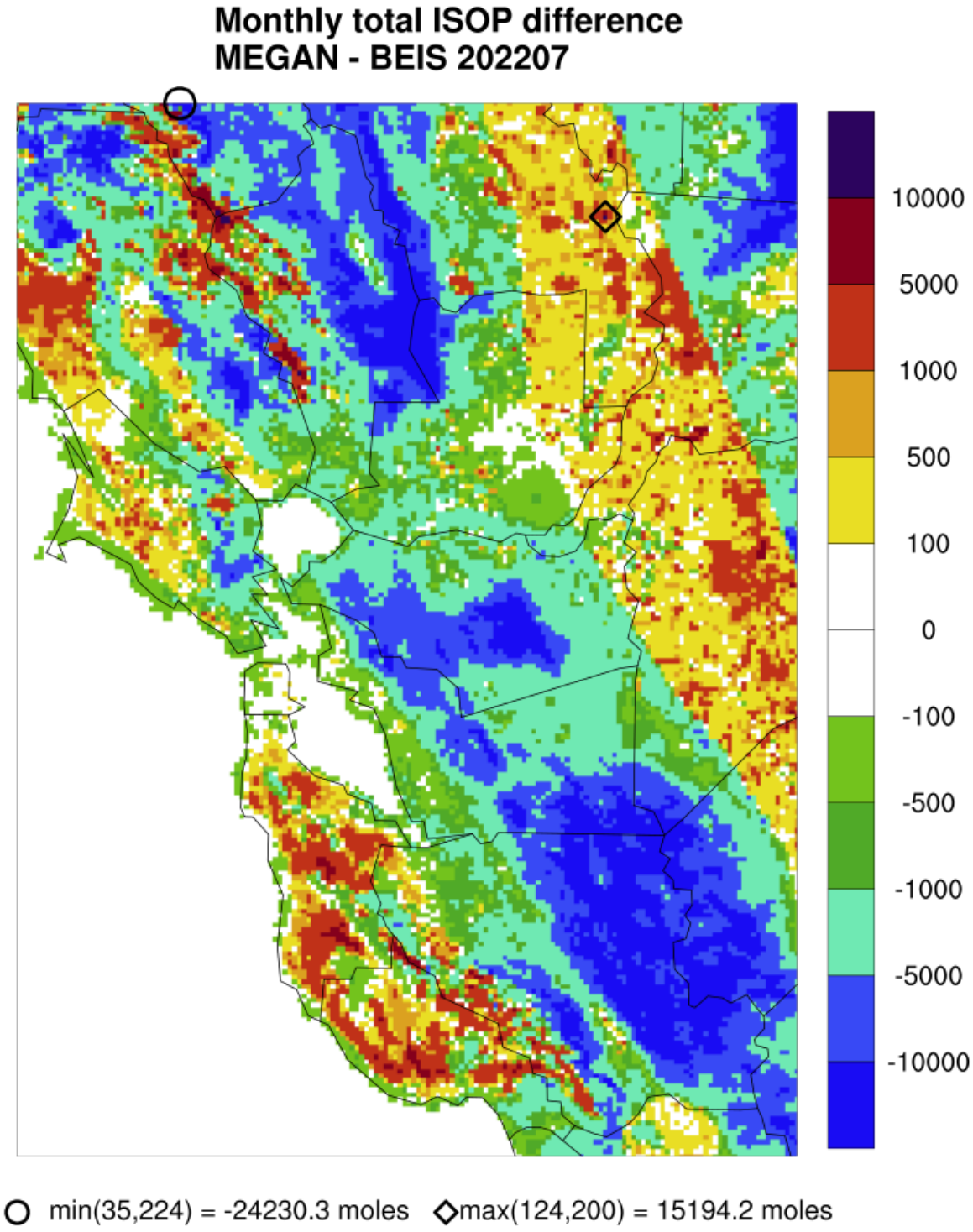

Figure 3-6. Differences between total MEGAN and BEIS emissions (in moles) of isoprene in July 2022.

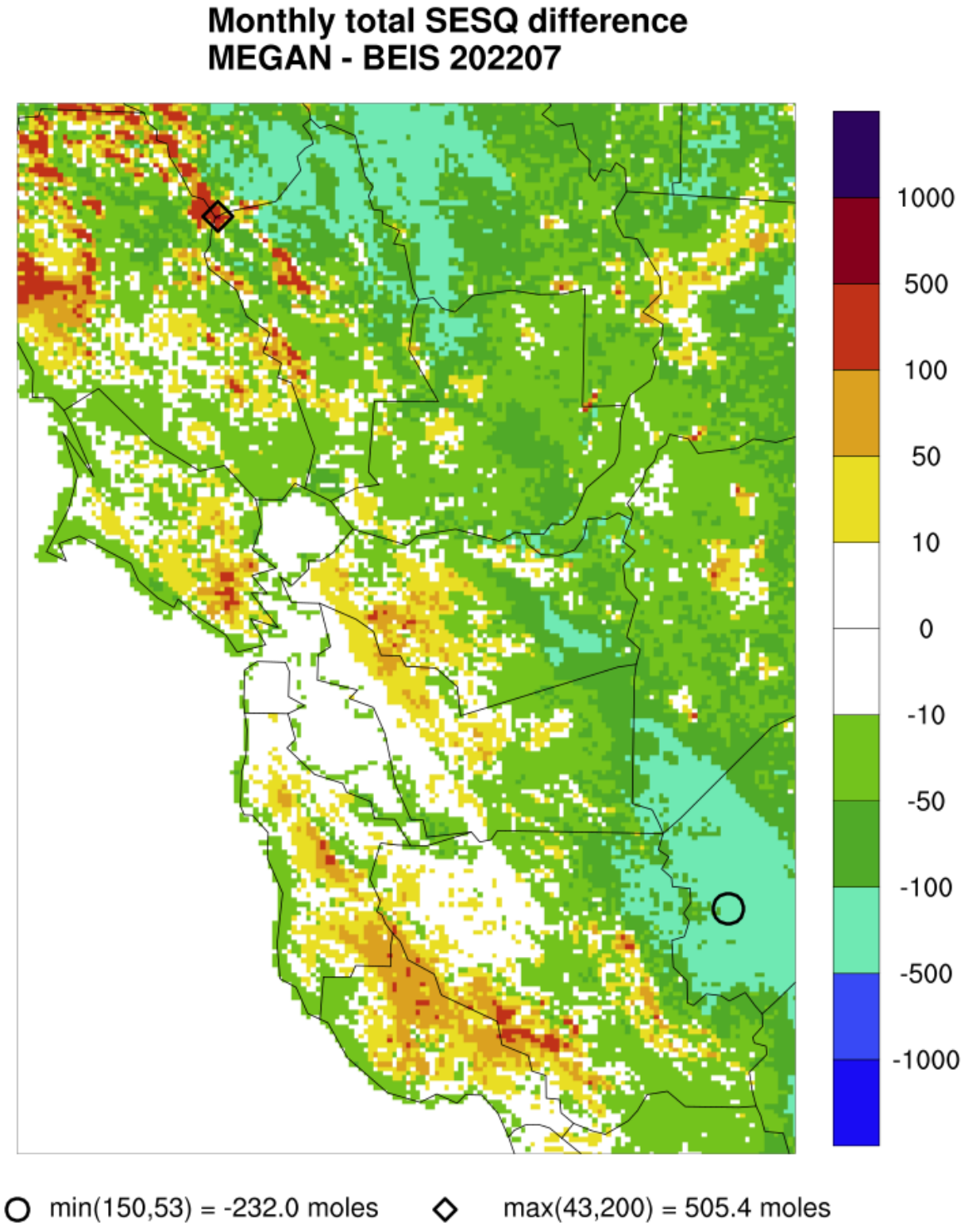

Figure 3-7. Differences between total MEGAN and BEIS emissions (in moles) of sesquiterpenes in July 2022.

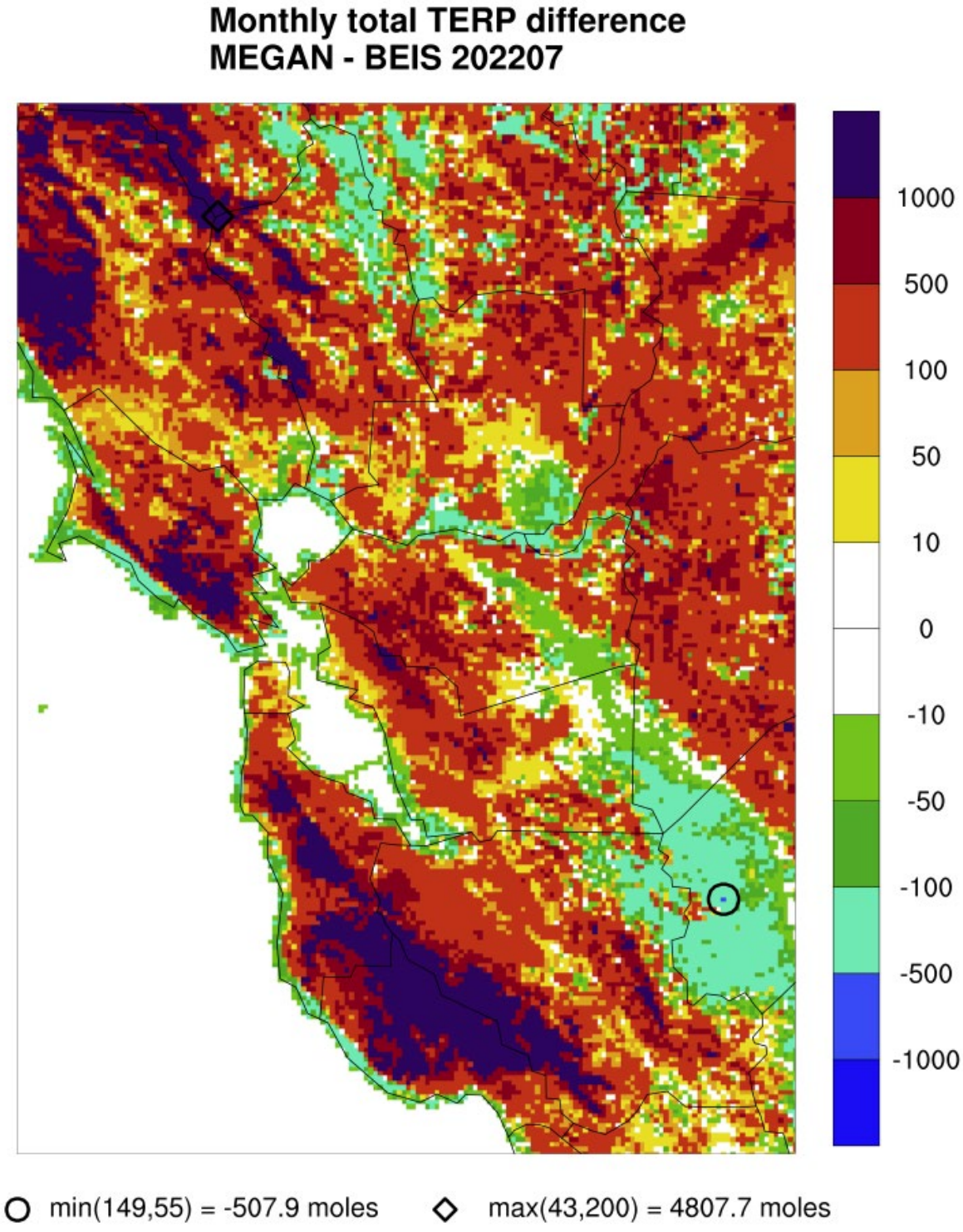

Figure 3-8. Differences between total MEGAN and BEIS emissions (in moles) of other terpenes in July 2022.

3.3 Model Performance for $PM_{2.5}$

The model performance evaluation compares CMAQ predicted $PM_{2.5}$ concentrations with measurement data from monitoring sites located throughout the Bay Area (Figure 3-9). All sites measure total $PM_{2.5}$ mass according to Federal Reference Methods (FRM) or Federal Equivalent Methods (FEM). A single site in San Jose (Jackson Street) is a Chemical Speciation Network (CSN) monitor that measures speciated particulate components, including sulfate, particulate nitrate (hereafter referred to as nitrate), ammonium, elemental and organic carbon, sea salt, and crustal (dust) elements.

3.3.1 Model Performance for Total $PM_{2.5}$

Figure 3-10 shows two important statistical measures of model performance, the normalized mean bias (NMB) and the normalized mean error (NME) in model predictions of total $PM_{2.5}$. The boxes in the figure represent statistical benchmarks for historically well-performing models (Emery et al., 2017). Such plots are often referred to as soccer plots, since the boxes are in the shape of a soccer goal. Each symbol in the plot represents the aggregate statistic across all monitoring sites. Results are shown for the reference case (SAPRC07/AERO7 with MEGAN emissions), and the 3 SAPRC-22 configurations: SAPRC-22/AERO6.8 with BEIS emissions, SAPRC-22-VCP/AERO6.8 with BEIS emissions, and SAPRC-22-VCP/AERO6.8 with MEGAN emissions. All configurations over-predict $PM_{2.5}$ during the winter months. However, the over-prediction bias is higher for the three SAPRC-22 configurations than for the SAPRC07 configuration. Treating VCPs explicitly has a negligible impact on model performance with the SAPRC-22 mechanism (Figure 3-10b and Figure 3-10c). Using MEGAN instead of BEIS for BVOC emissions also has a generally negligible impact on model performance, with a small improvement in over-prediction bias in December (Figure 3-10c and Figure 3-10d). The negligible to small differences in model performance between the two BVOC models are consistent with a previous Air District Study using SAPRC07 (Guenther et al., 2025). The results with the 3 SAPRC-22 configurations show a small improvement in underprediction bias in the spring months (April and May) as compared to the reference SAPRC07 configuration. Figure 3-11 shows the soccer plots for annual $PM_{2.5}$ performance by monitoring site. The results show that the over-prediction bias in annual $PM_{2.5}$ increases for most sites when the SAPRC-22 chemistry option is selected as compared to the SAPRC07 option.

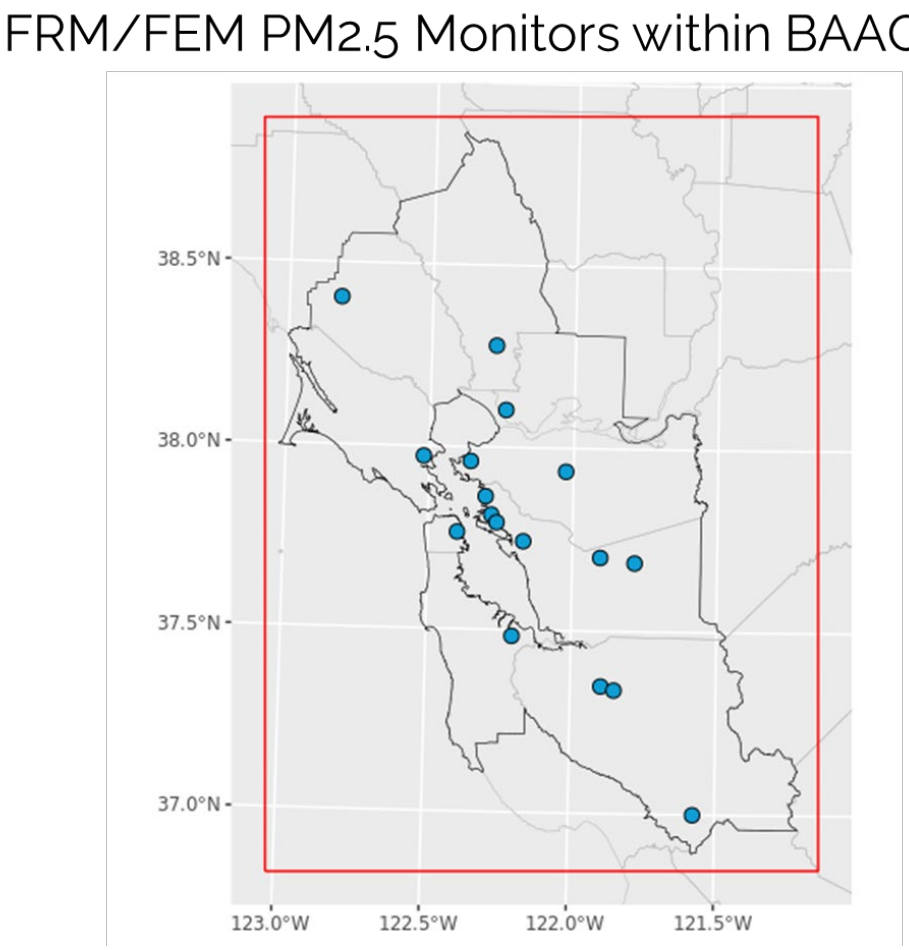

Figure 3-9. Locations of the Air District's PM monitoring sites within its jurisdiction, shown by the black outline that generally follows the 9-county boundaries. The Bay Area 1 km grid is indicated by the red box.

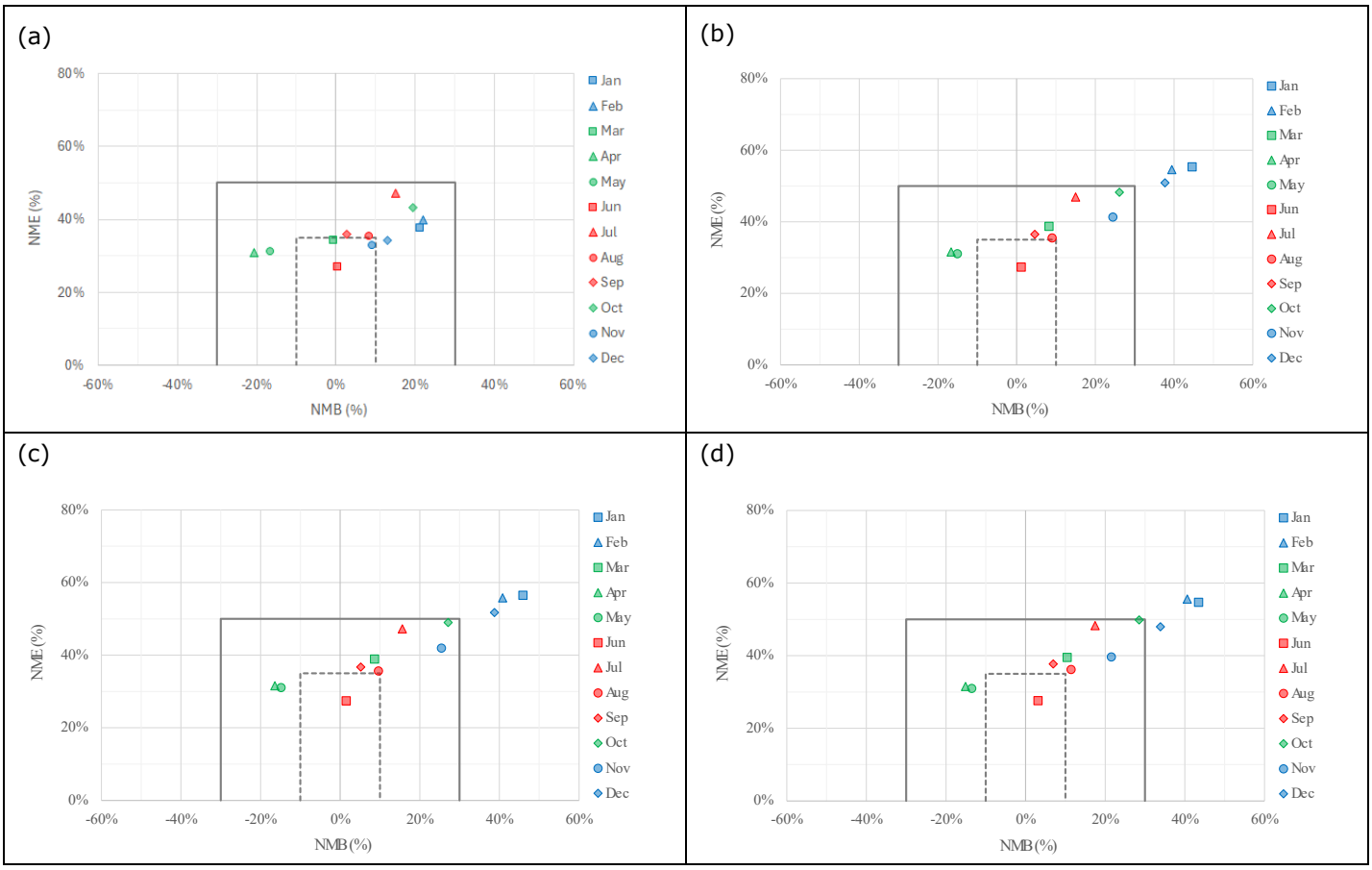

Figure 3-10. Soccer plots of $PM_{2.5}$ model performance by month (across all sites) for (a) SAPRC07-AERO7-MEGAN, (b) SAPRC-22-AERO68-BEIS, (c) SAPRC-22-VCP-AERO68-BEIS, and (d) SAPRC-22-VCP-AERO68-MEGAN.

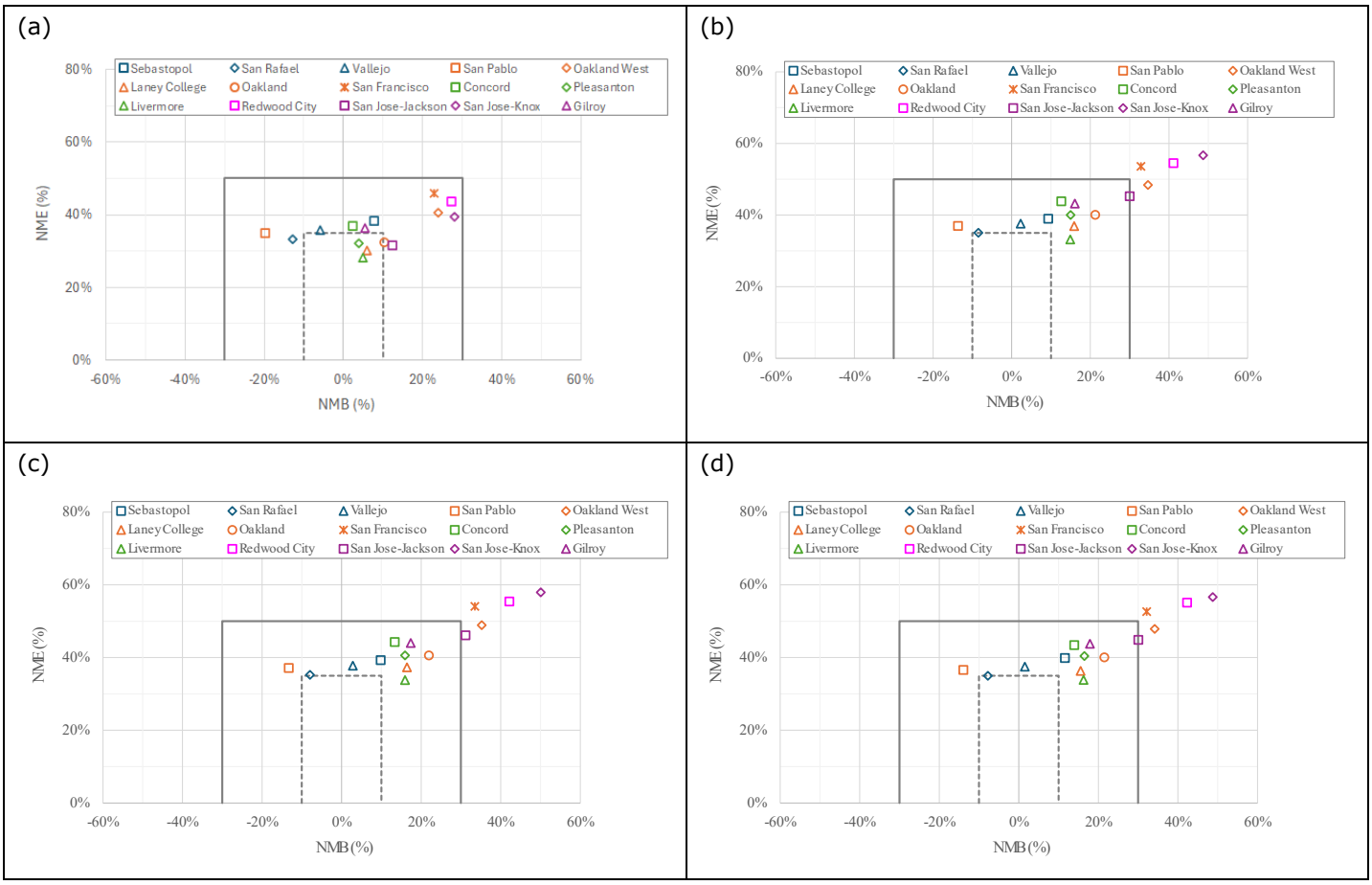

Figure 3-11. Soccer plots of annual $PM_{2.5}$ model performance by monitoring site for (a) SAPRC07-AERO7-MEGAN, (b) SAPRC-22-AERO68-BEIS, (c) SAPRC-22-VCP-AERO68-BEIS, and (d) SAPRC-22-VCP-AERO68-MEGAN.

3.3.2 Model Performance for Speciated $PM_{2.5}$

Figure 3-12 shows the seasonal and annual NMB in predicted $PM_{2.5}$ sulfate concentrations at the single CSN site (San Jose-Jackson). Winter months include January, February, November, and December while summer spans June through September. The remaining months are grouped into spring/fall. Results are shown for the SAPRC07 reference case and the three SAPRC-22 configurations tested in this study. The differences in NMB are negligible for all 4 model configurations, indicating that the changes in model chemistry and/or biogenic emissions estimates do not significantly affect $PM_{2.5}$ sulfate.

Figure 3-13 shows the NMB results for $PM_{2.5}$ nitrate from the 4 model configurations. Compared to the reference case with SAPRC07, all 3 SAPRC-22 configurations show higher nitrate predictions. There is a large increase in the over-estimation bias during the winter months, and a smaller but still significant increase in the spring/fall months and in the annual values. In the summer, the NMB changes from a slight underprediction with SAPRC07 to a slight overprediction with the SAPRC-22 configurations.

The NMB results for $PM_{2.5}$ organic carbon (OC) mass are shown in Figure 3-14. As in the case of $PM_{2.5}$ components such as nitrate and ammonium, the three SAPRC-22 simulations predict higher OC values than the SAPRC07 simulation. This leads to a change from a slight underprediction in the winter months in the SAPRC07 simulation to a large overprediction in the SAPRC-22 simulations, improvement from a large underprediction to a small underprediction in the spring/fall months, and a change from a slight underprediction to a small but non-negligible overprediction in the annual value.

3.3.3 Discussion of model performance

The model performance results show that all configurations of CMAQ with SAPRC-22 chemistry predict higher total $PM_{2.5}$ concentrations than the reference case with SAPRC07 chemistry. This leads to large overpredictions in most cases with some improvements when SAPRC07 underpredicts $PM_{2.5}$ concentrations. The differences between SAPRC-22 results and SAPRC07 results are largest in winter and smallest in summer, with the spring/fall months in between these extremes. Significantly more $PM_{2.5}$ nitrate is produced in the winter in the SAPRC-22 simulations than in the SAPRC07 reference case. Organic carbon predictions are also much higher in winter in the SAPRC-22 simulations than in the SAPRC07 simulation. Differences among the three SAPRC-22 simulations are negligible, indicating that the SAPRC-22 gas-phase chemistry drives the differences in model results from the reference SAPRC07 case.

Figure 3-15, Figure 3-16, and Figure 3-17 show the MDA8 ozone values over the modeling domain for a winter month (January), a spring month (April), and a summer month (July), respectively. Since the results from all SAPRC-22 simulations were similar, we only show the comparison between the SAPRC07 reference and the SAPRC-22 simulation with VCP chemistry and with MEGAN emissions. The figures also show the differences in MDA8 ozone between the SAPRC07 and SAPRC-22 simulations. As seen in the figures, the simulation with SAPRC-22 predicts substantially higher ozone in winter, with smaller differences in the spring month, and even smaller differences in the summer month.

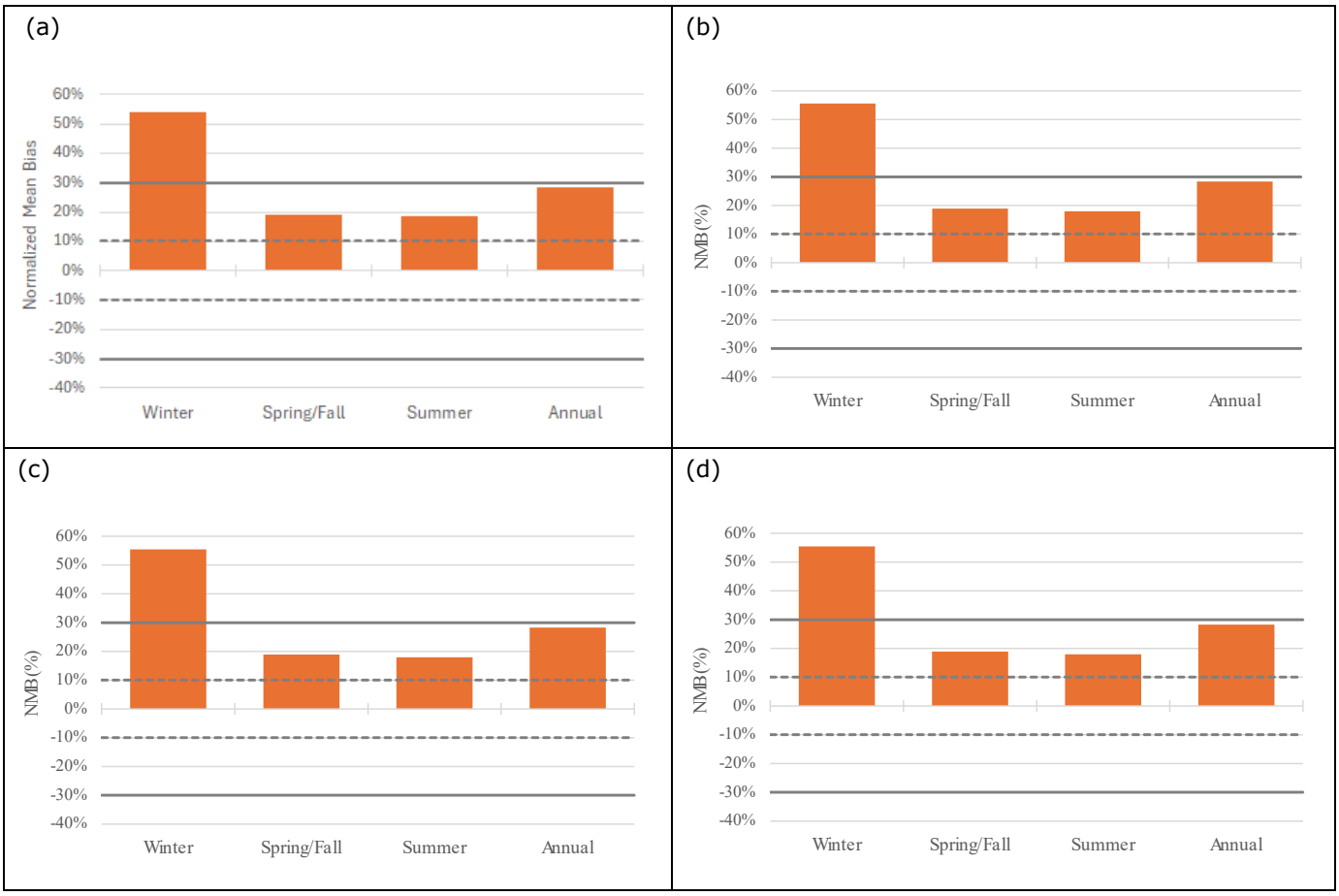

Figure 3-12. NMB in seasonal and annual $PM_{2.5}$ sulfate at the San Jose-Jackson CSN monitor for (a) SAPRC07-AERO7-MEGAN, (b) SAPRC-22-AERO68-BEIS, (c) SAPRC-22-VCP-AERO68-BEIS, and (d) SAPRC-22-VCP-AERO68-MEGAN.

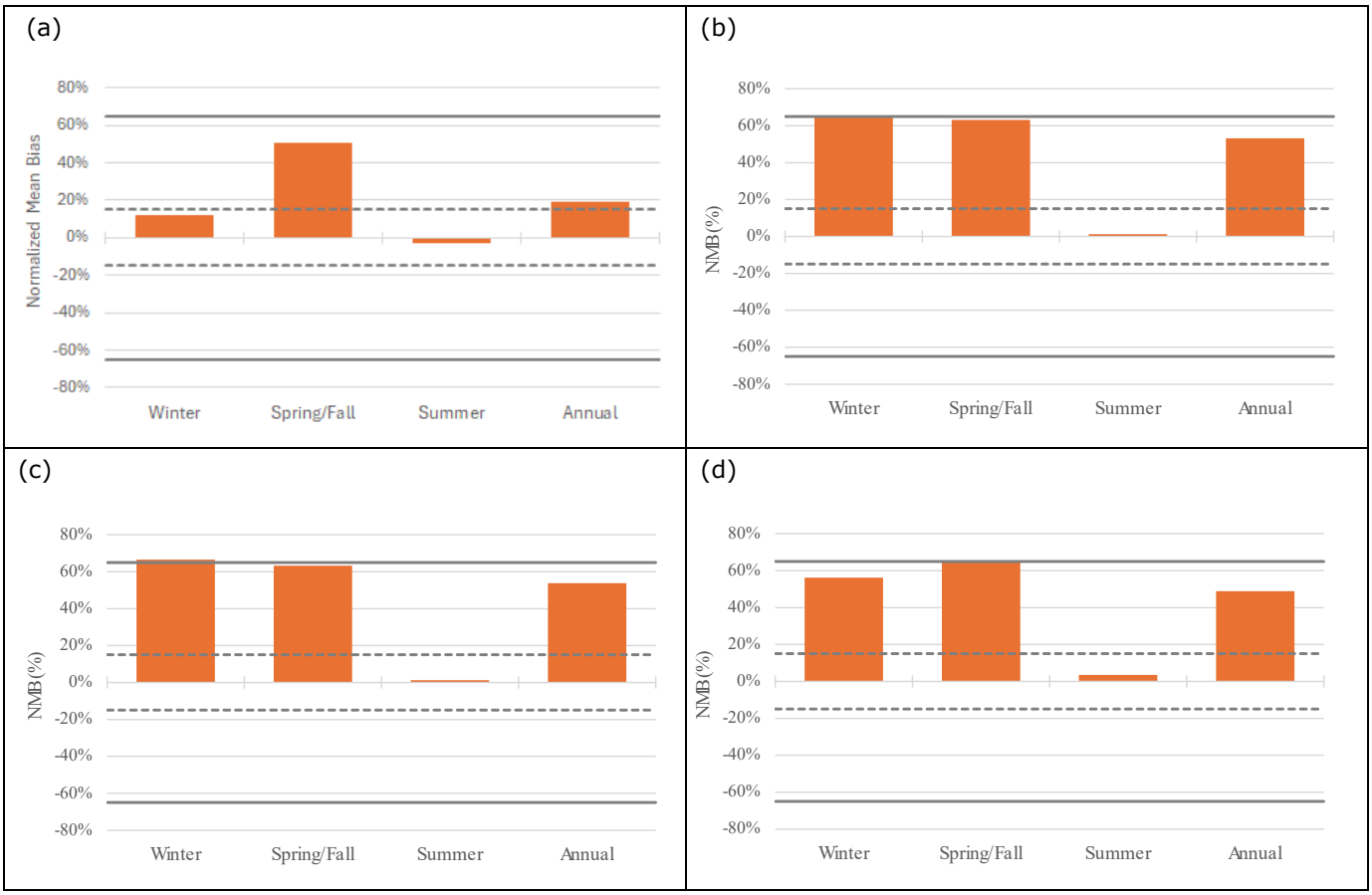

Figure 3-13. NMB in seasonal and annual $PM_{2.5}$ nitrate at the San Jose-Jackson CSN monitor for (a) SAPRC07-AERO7-MEGAN, (b) SAPRC-22-AERO68-BEIS, (c) SAPRC-22-VCP-AERO68-BEIS, and (d) SAPRC-22-VCP-AERO68-MEGAN.

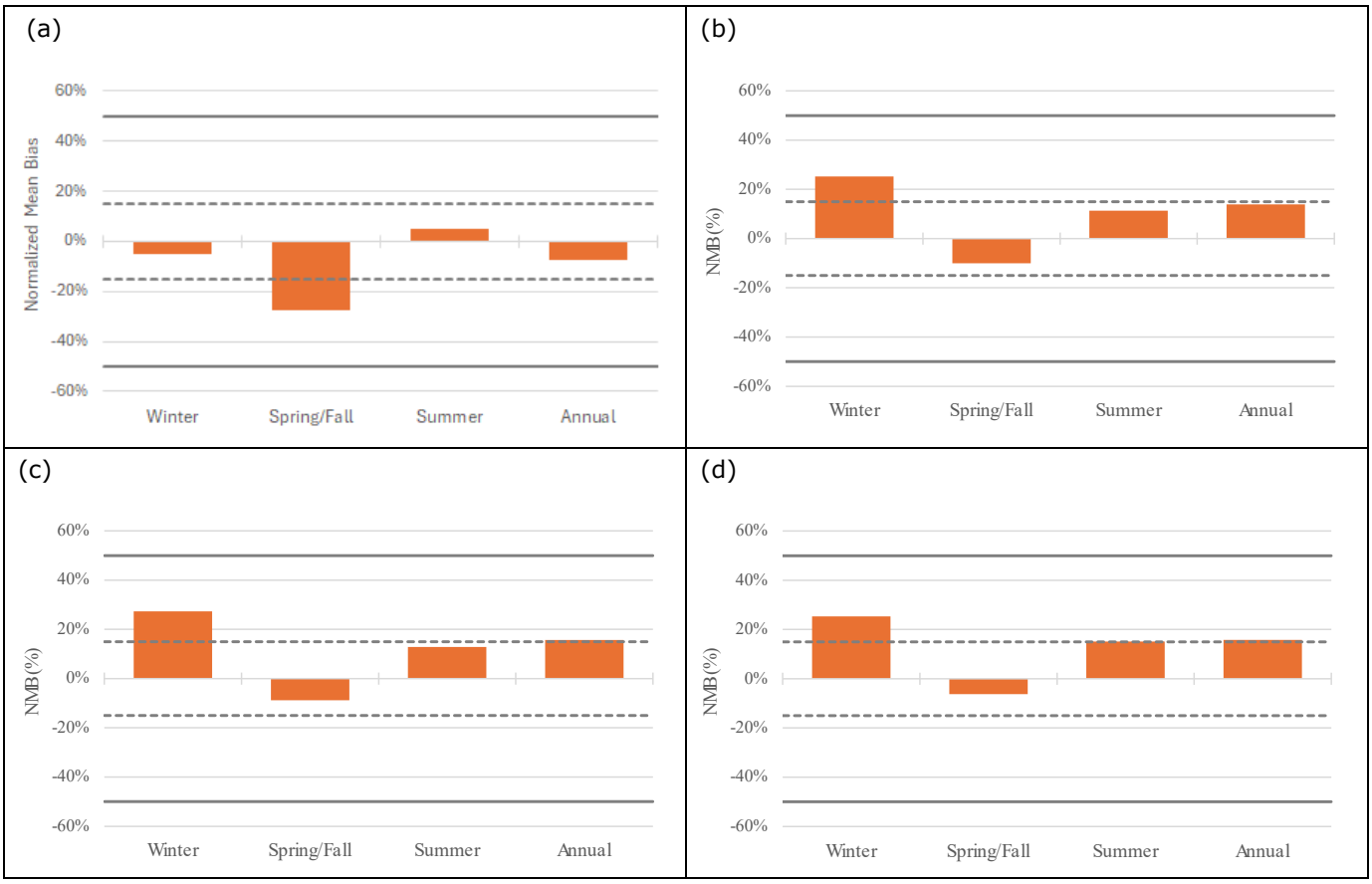

Figure 3-14. NMB in seasonal and annual $PM_{2.5}$ organic carbon at the San Jose-Jackson CSN monitor for (a) SAPRC07-AERO7-MEGAN, (b) SAPRC-22-AERO68-BEIS, (c) SAPRC-22-VCP-AERO68-BEIS, and (d) SAPRC-22-VCP-AERO68-MEGAN.

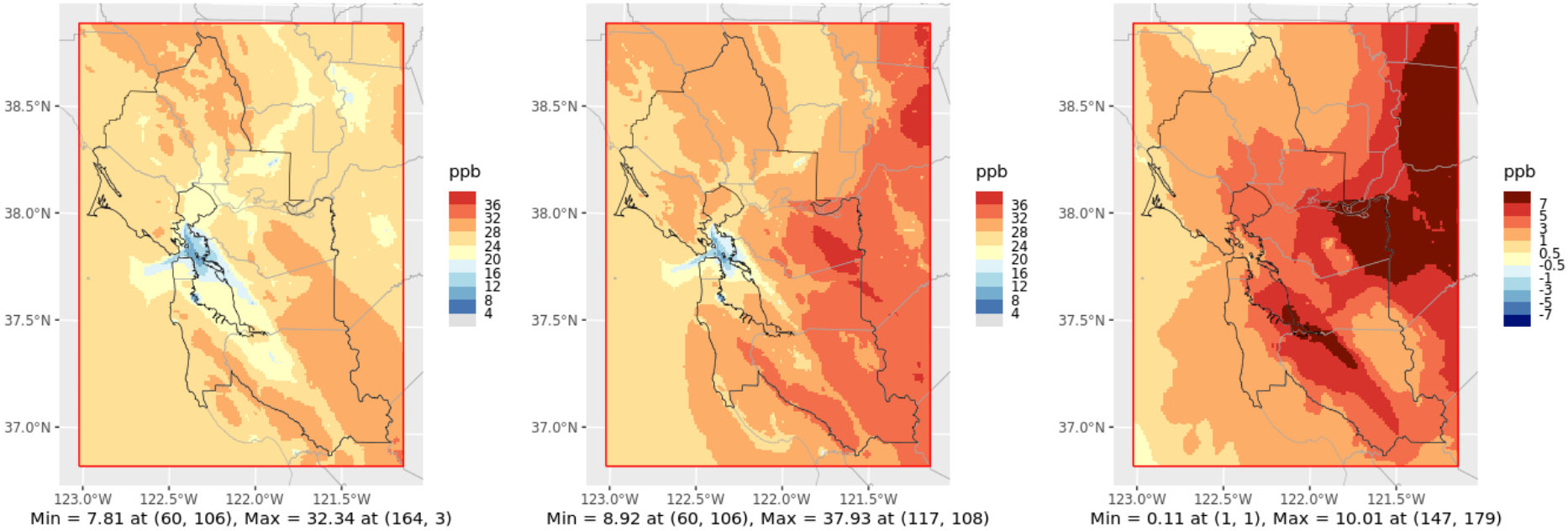

Figure 3-15. Monthly average MDA8 ozone in January: SAPRC07 chemistry (left), SAPRC-22 chemistry (middle), SAPRC-22 – SAPRC07 (right).

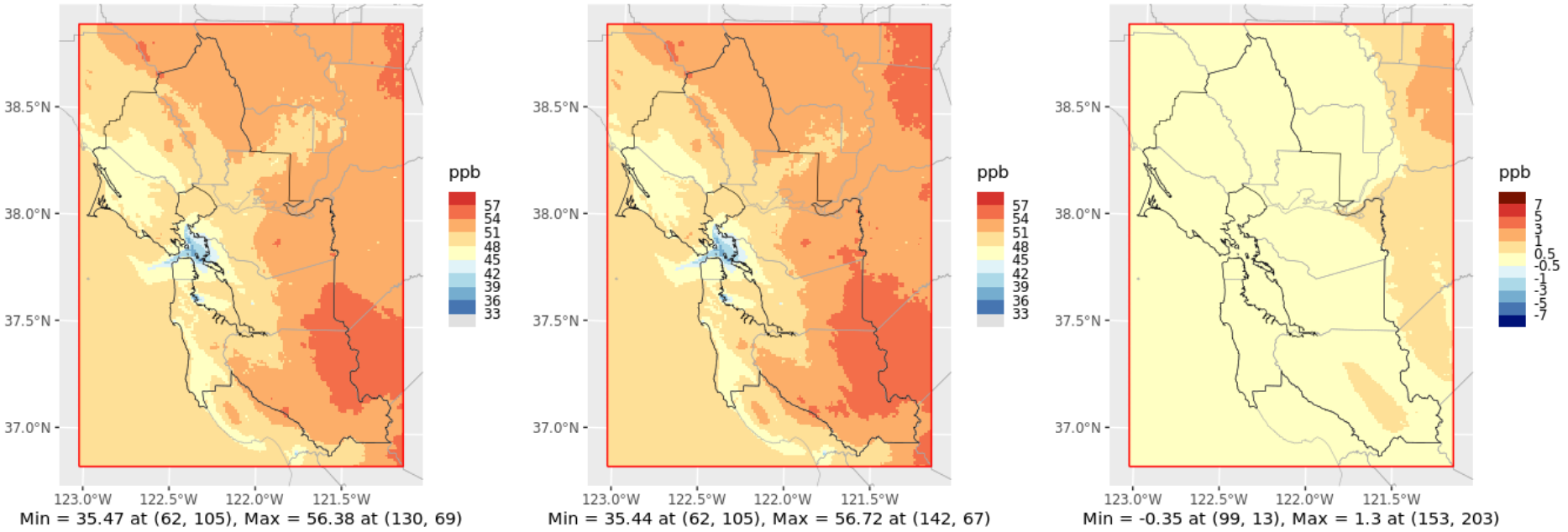

Figure 3-16. Monthly average MDA8 ozone in April: SAPRC07 chemistry (left), SAPRC-22 chemistry (middle), SAPRC-22 – SAPRC07 (right).

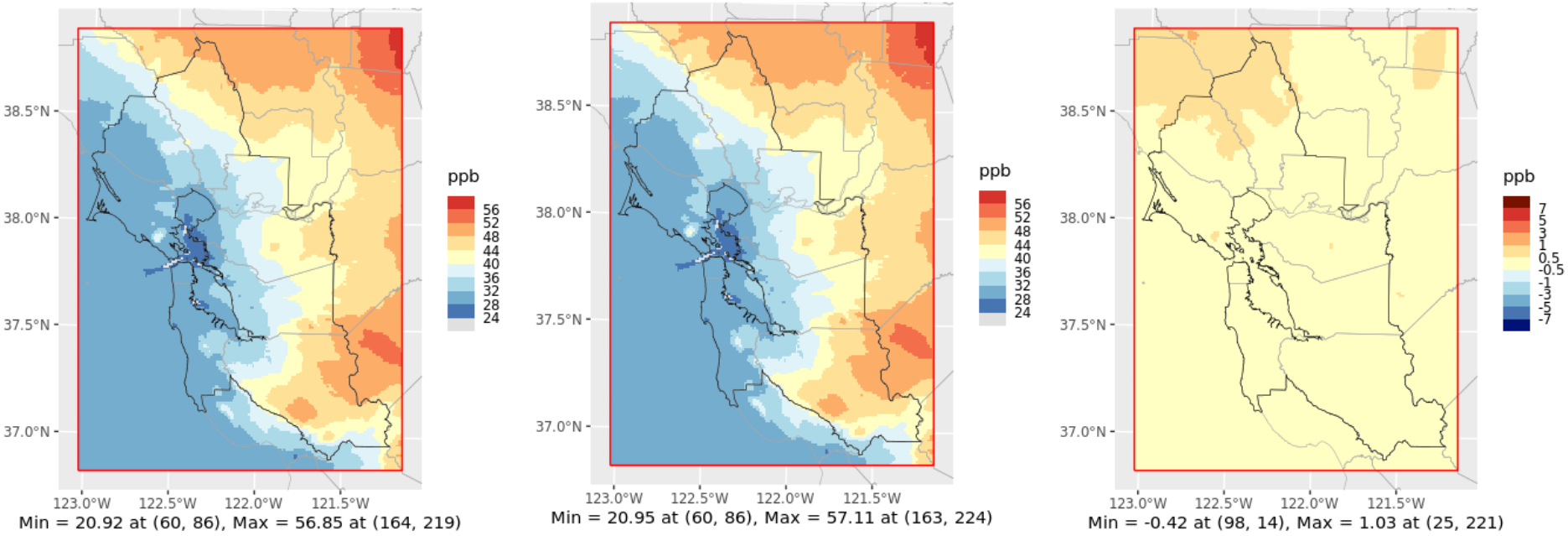

Figure 3-17. Monthly average MDA8 ozone in July: SAPRC07 chemistry (left), SAPRC-22 chemistry (middle), SAPRC-22 – SAPRC07 (right).

The much higher winter ozone predictions, and the smaller summer differences using SAPRC-22 chemistry are consistent with the $PM_{2.5}$ results. Since nighttime NO_3 radical chemistry plays a much larger role in the formation of $PM_{2.5}$ nitrate, SOA, and ozone in the winter months than in the summer months, these results suggest that the differences between the two mechanisms are influenced by differences in their treatment of NO_3 reactions. Higher O_3 concentrations in the SAPRC-22 simulations also increase the oxidation chemistry, which enhances the formation of $PM_{2.5}$.

4.0 EMISSION SCENARIOS

The Air District conducted multiple emission scenarios to test the response of CMAQ with SAPRC-22-VCP chemistry and MEGAN biogenic emissions to changes in NOx and VOC anthropogenic emissions. The Air District selected the scenarios after consulting with Ramboll.

The Air District conducted the following 4 emission control scenarios for a winter month (January), spring/fall month (April), and a summer month (July):

1. 20% reduction in anthropogenic VOC emissions
2. 40% reduction in anthropogenic VOC emissions
3. 40% reduction in anthropogenic NOx emissions
4. 40% reduction in anthropogenic NOx and VOC emissions

Ramboll processed and analyzed the speciated 24-hour average $PM_{2.5}$ outputs of the emission scenarios simulation provided by the Air District for each of the 3 months. The full list of outputs provided by the Air District is shown in Table 4-1 below:

Table 4-1. List of $PM_{2.5}$ variables provided for analysis.

Variable	**Variable Name**
Total $PM_{2.5}$ mass	ATOTIJ_RSS
$PM_{2.5}$ sulfate	PMF_SO4
$PM_{2.5}$ nitrate	PMF_NO3
$PM_{2.5}$ ammonium	PMF_NH4
$PM_{2.5}$ anthropogenic SOA	PMF_ASOA
$PM_{2.5}$ biogenic SOA	PMF_BSOA
$PM_{2.5}$ SOA from glyoxal/methylglyoxal	PMF_CLDGLY
$PM_{2.5}$ POA	PMF_POA
$PM_{2.5}$ elemental carbon	PMF_EC
$PM_{2.5}$ sodium	PM25_NA
$PM_{2.5}$ chloride	PM25_CL

The impacts on $PM_{2.5}$ sulfate, elemental carbon, sodium, chloride, and POA were negligible to very small. $PM_{2.5}$ SOA produced in clouds from glyoxal/methylglyoxal is a very small fraction of total SOA and the changes in this component due to the emission reductions were also small. Thus, our discussion focuses on the remaining $PM_{2.5}$ variables in Table 4-1.

Figure 4-1 shows the base case monthly average $PM_{2.5}$ anthropogenic SOA concentrations for January, and the effects of the 4 emissions reductions scenarios on the monthly average values. VOC reductions result in SOA decreases as expected, while NOx reductions lead to increases in anthropogenic SOA over most of the domain. The combined 40% VOC-NOx reduction scenario also results in decreases in anthropogenic SOA, but the decreases are smaller than the decreases in either of the VOC-only reduction scenarios because of the NOx reduction offset. The largest decreases (and increases in the case of the NOx reduction scenario) are in Alameda and Santa Clara Counties, suggesting that the region is VOC-limited.

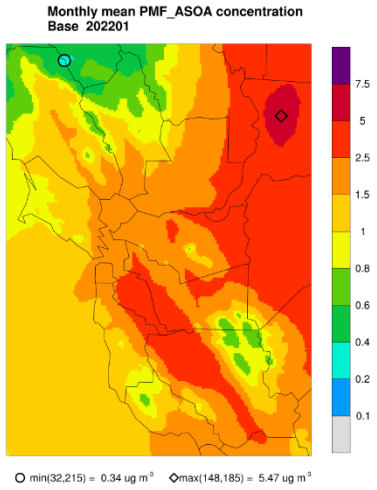

Monthly Average Anthropogenic SOA

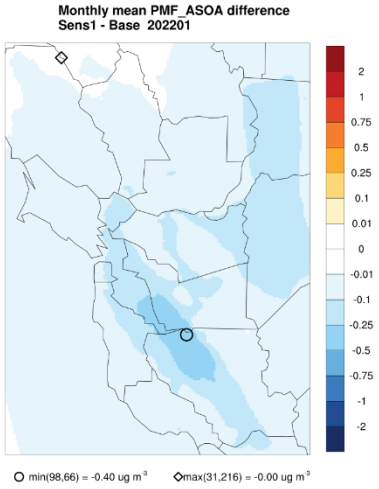

20% VOC Reduction

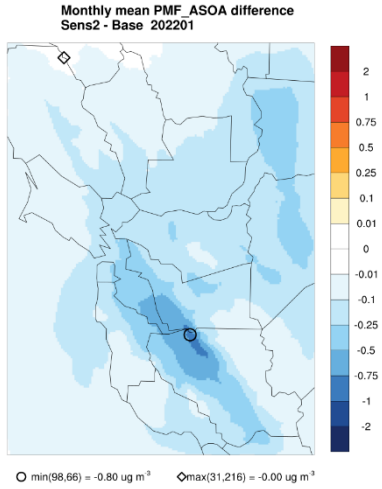

40% VOC Reduction

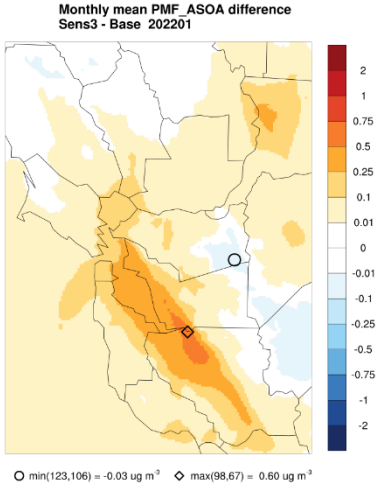

40% NOx Reduction

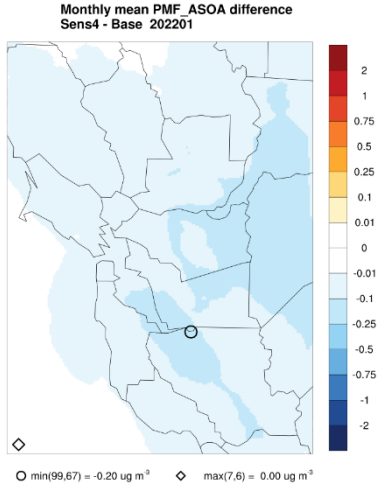

40% VOC & NOx Reduction

Figure 4-1. January average $PM_{2.5}$ anthropogenic SOA and responses to emissions reductions.

Possible reasons for the increases in anthropogenic SOA when NOx emissions are reduced include:

- Under VOC-limited conditions (high NOx areas and low VOC areas), reducing NOx can increase oxidant levels because NOx "scavenges" radicals like OH and HO_2 that would otherwise oxidize VOCs (e.g., Wang et al., 2024; Chen et al., 2022).
- SOA yields from most anthropogenic SOA precursors, such as aromatics and alkanes, are higher under low NOx conditions than under high NOx conditions (e.g., Song et al., 2005; Ng et al., 2007a; Lane et al., 2008; Li et al., 2019; Wang et al., 2021, Hallward-Driemeier et al., 2024).

From Figure 4-2, which shows the base case monthly average $PM_{2.5}$ biogenic SOA concentrations for January, and the responses to emission reductions, we see that anthropogenic VOC reductions also cause a decrease in biogenic SOA. NOx reductions lead to both increases and decreases in biogenic SOA. The combined 40% VOC-NOx reduction scenario results in decreases in biogenic SOA. The largest decreases (and increases in the case of the NOx reduction scenario) are in Alameda and Santa Clara Counties for the VOC reduction and the NOx reduction scenarios, and in San Joaquin County for the combined VOC and NOx reduction scenarios. The increases in biogenic SOA in some areas in response to NOx reductions can again be attributed to both the scavenging of oxidants and the lower SOA yields from isoprene (e.g., Kroll et al., 2006), monoterpenes such as α-pinene and β-pinene (e.g., Ng et al., 2007b; Pullinen et al., 2020; Wang et al., 2024; Liu et al., 2025). However, as noted by Ng et al. (2007b), the NOx dependence of SOA yield for sesquiterpenes differs from that determined for isoprene and α-pinene; their aerosol yield under high-NOx conditions substantially exceeds that under low-NOx conditions. The decreases in biogenic SOA in response to anthropogenic VOC emissions reductions are likely due to decreased levels of oxidants and to reductions in available surface area for condensation of biogenic SOA.

Figure 4-3 shows the January average base case $PM_{2.5}$ organic carbon mass and the changes in OC mass in response to the 4 emission reduction scenarios. As noted previously, the impacts of the emission reductions on POA are small, so the impacts on OC reflect the results for the anthropogenic and biogenic SOA components discussed above.

The results for $PM_{2.5}$ nitrate and ammonium are shown in Figure 4-4 and Figure 4-5, respectively. As shown in Figure 4-4, reducing VOC emissions results in generally lower $PM_{2.5}$ nitrate, but there are small increases in a few areas. NOx and combined VOC-NOx reductions result in decreases everywhere in $PM_{2.5}$ nitrate. Decreasing VOC emissions lowers the daytime production of nitrate but nitrate radical levels can be higher at night when VOC emissions are reduced, leading to some nocturnal production of nitrate, possibly explaining the small increases in $PM_{2.5}$ nitrate with VOC reductions. From Figure 4-5, we see that $PM_{2.5}$ ammonium decreases in all 4 emission scenarios.

Figure 4-6 shows the results for total $PM_{2.5}$ concentrations. While total $PM_{2.5}$ is generally reduced in all 4 emission reduction scenarios, there are some increases (NOx disbenefit) predicted in the NOx reduction scenario. These increases coincide with the increases in anthropogenic and biogenic SOA shown in Figure 4-1 and Figure 4-2, respectively.

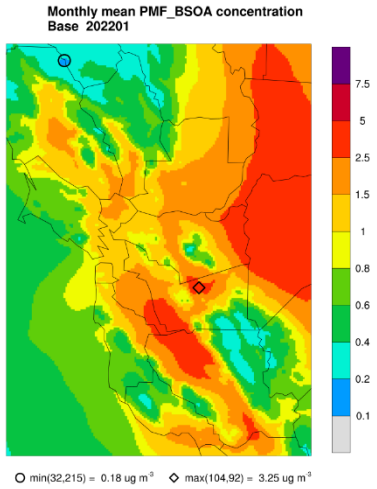

Monthly Average Biogenic SOA

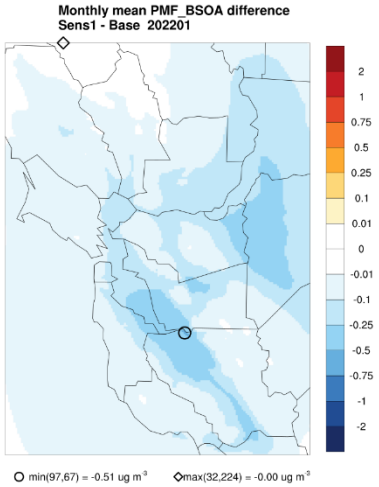

20% VOC Reduction

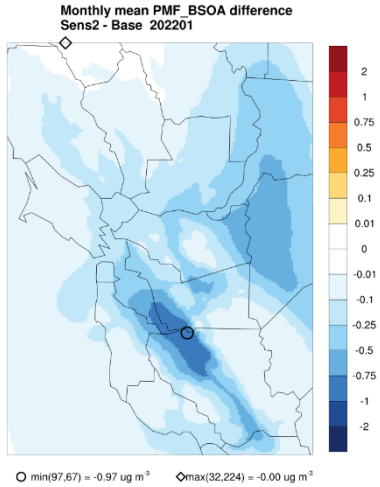

40% VOC Reduction

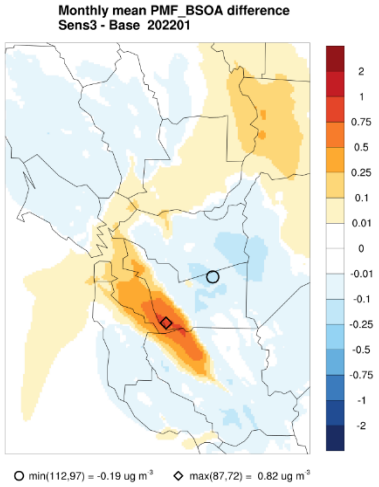

40% NOx Reduction

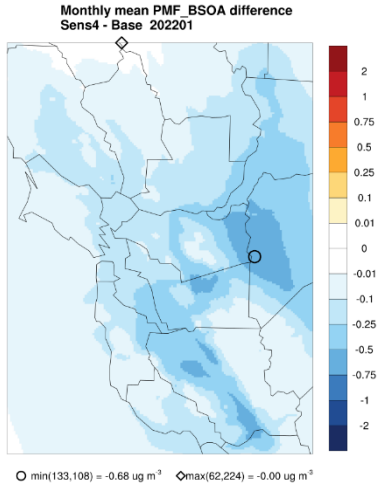

40% VOC & NOx Reduction

Figure 4-2. January average $PM_{2.5}$ biogenic SOA and responses to emissions reductions.

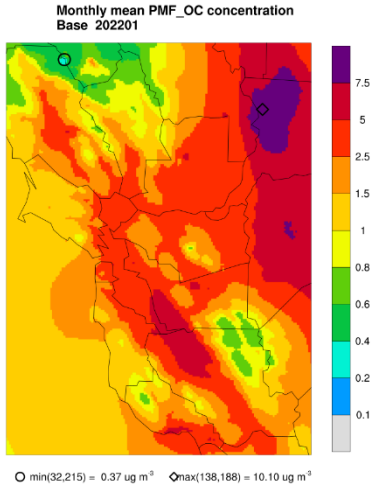

Monthly Average OC Mass

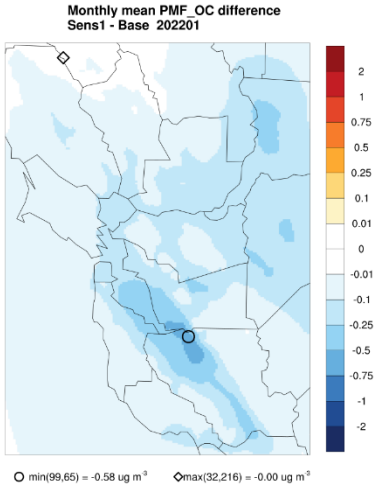

20% VOC Reduction

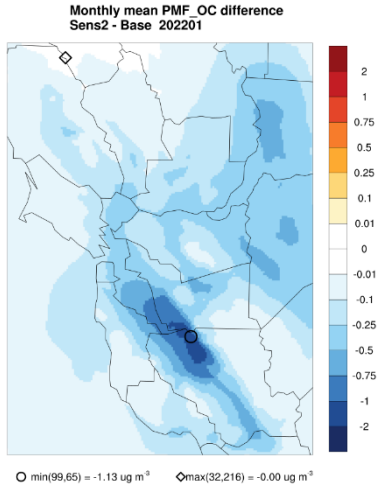

40% VOC Reduction

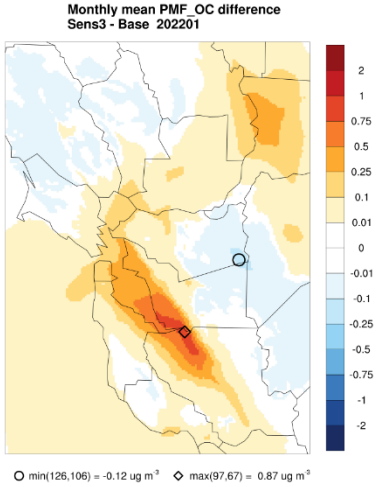

40% NOx Reduction

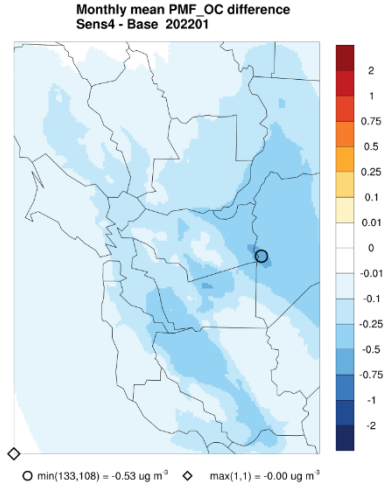

40% VOC & NOx Reduction

Figure 4-3. January average $PM_{2.5}$ organic carbon (OC) mass and responses to emissions reductions.

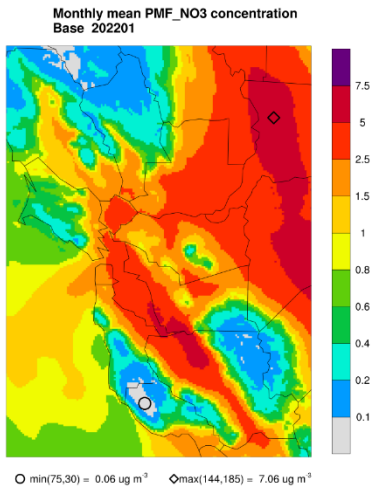

Monthly Average $PM_{2.5}$ Nitrate

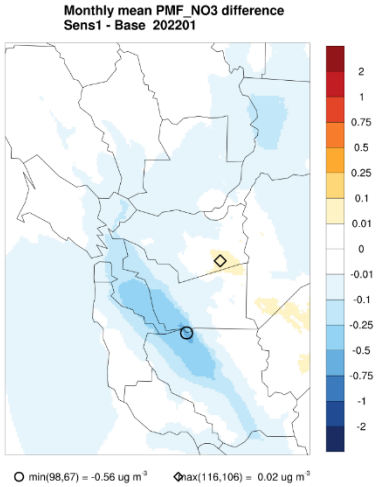

20% VOC Reduction

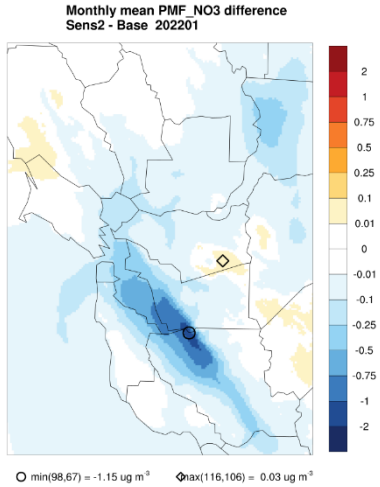

40% VOC Reduction

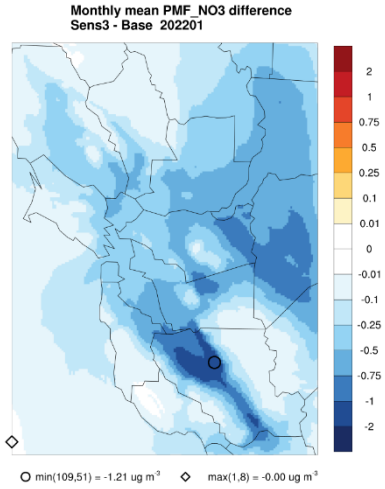

40% NOx Reduction

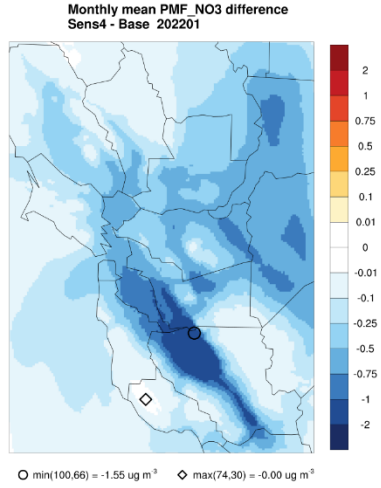

40% VOC & NOx Reduction

Figure 4-4. January average $PM_{2.5}$ nitrate and responses to emissions reductions.

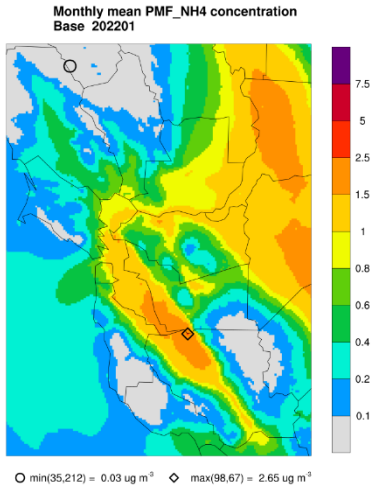

Monthly Average
$PM_{2.5}$ Ammonium

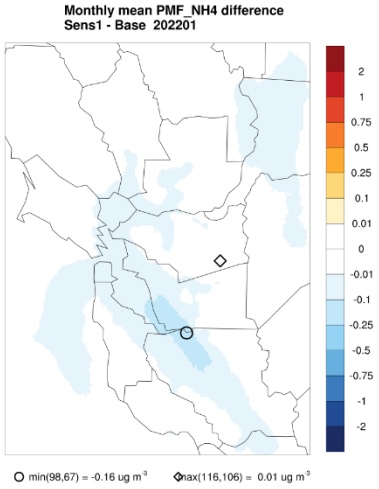

20% VOC Reduction

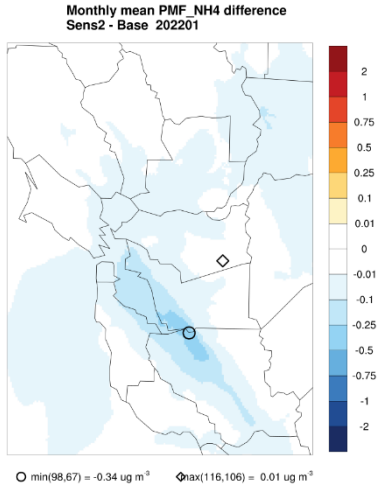

40% VOC Reduction

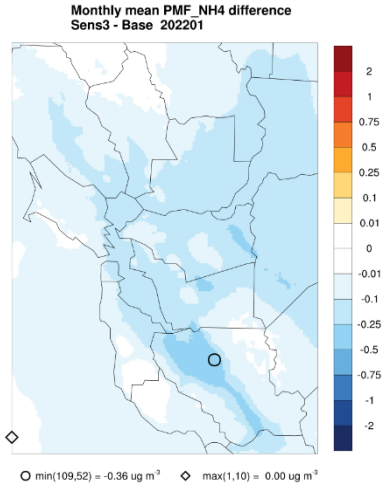

40% NOx Reduction

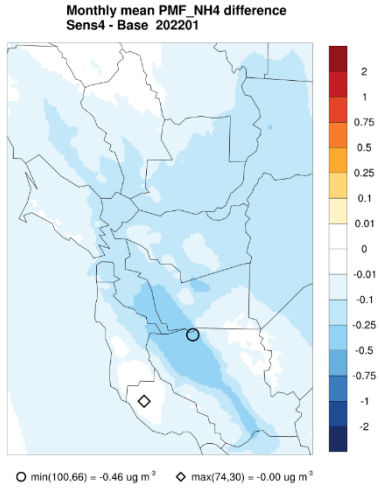

40% VOC & NOx Reduction

Figure 4-5. January average $PM_{2.5}$ ammonium and responses to emissions reductions.

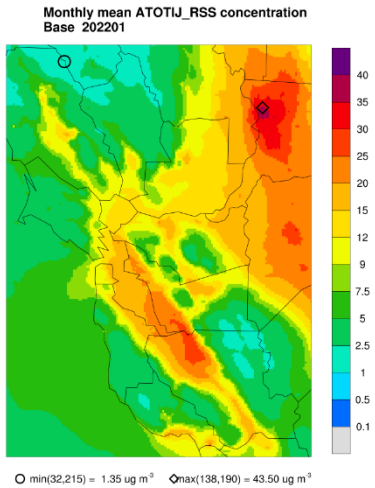

Monthly Average Total $PM_{2.5}$

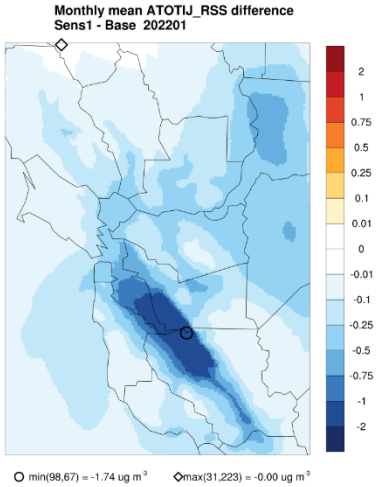

20% VOC Reduction

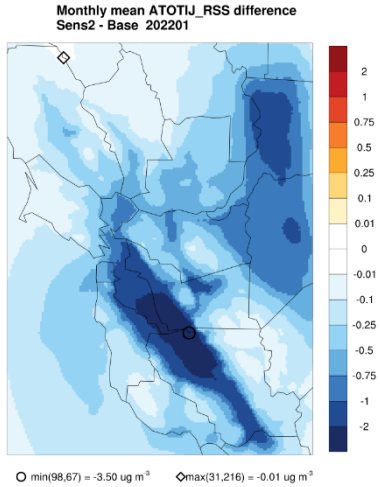

40% VOC Reduction

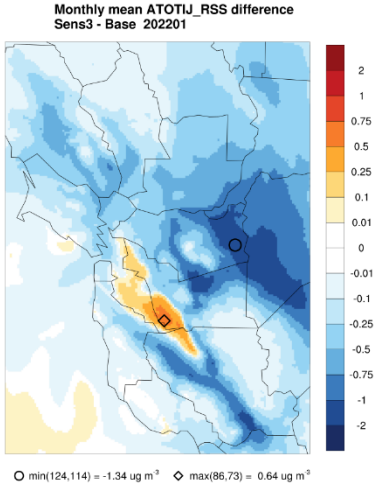

40% NOx Reduction

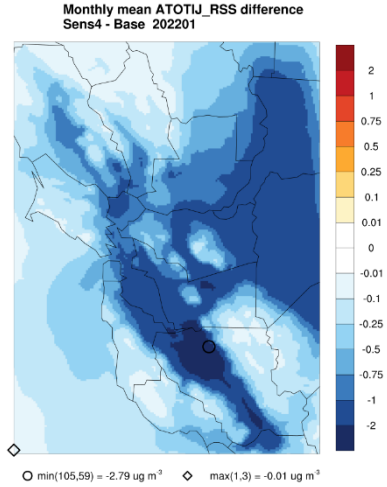

40% VOC & NOx Reduction

Figure 4-6. January average total $PM_{2.5}$ and responses to emissions reductions.

The results for the 2 other months (April and July) for which emission reduction scenarios were simulated are generally similar to those for January, with a few exceptions. $PM_{2.5}$ responses to the emission reductions are smaller in both April and July than in January. The increases in anthropogenic and biogenic SOA in April in response to NOx reductions are widespread but are much smaller than the increases in January, so the NOx disbenefit seen in April for total $PM_{2.5}$ is limited to a very small portion of the domain, as shown in Figure 4-7. In the summer month, the responses to the emission reductions are higher than in April but lower than in January. Figure 4-8 shows the total $PM_{2.5}$ in July and the changes in total $PM_{2.5}$ resulting from the emission reductions.

The larger impacts of the emissions reductions on total $PM_{2.5}$ in January as compared to the impacts in the spring and summer months are primarily associated with large impacts on SOA and nitrate. As discussed in Section 3, SOA is significantly overpredicted in winter than in the other seasons. This suggests that $PM_{2.5}$ responses in January to emissions reductions could possibly be smaller (on an absolute basis) than predicted due to the overestimation bias for SOA.

The anthropogenic emission scenarios discussed here show that biogenic SOA is affected by both VOC and NOx emission reductions (Figure 4-2). Changes in biogenic emissions are also likely to result in changes in model predictions of biogenic SOA and perhaps anthropogenic SOA. While this sensitivity simulation was not part of the scope of the work of this project, a future study could provide additional insight on the response of SOA to changes in biogenic emissions.

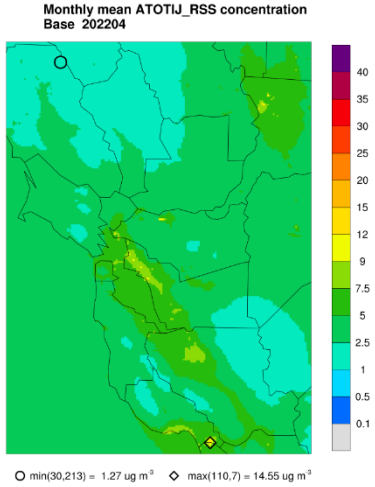

Monthly Average Total $PM_{2.5}$

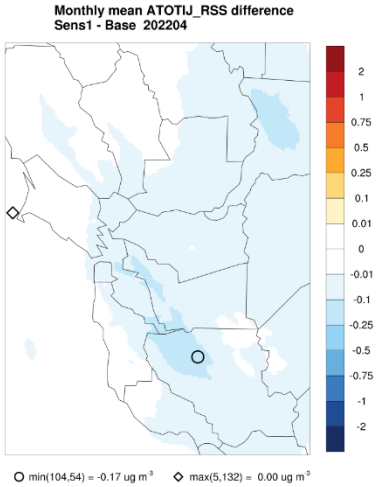

20% VOC Reduction

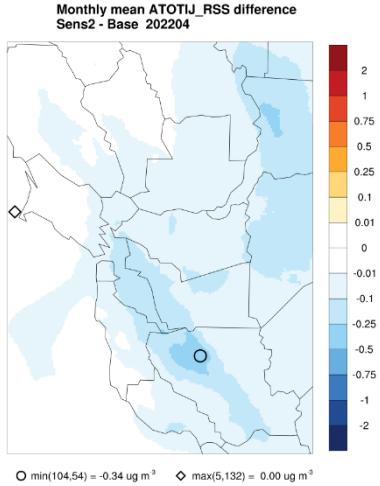

40% VOC Reduction

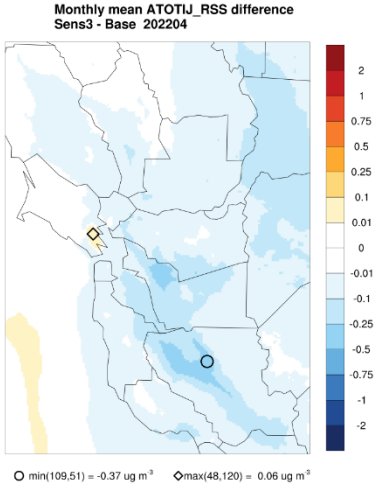

40% NOx Reduction

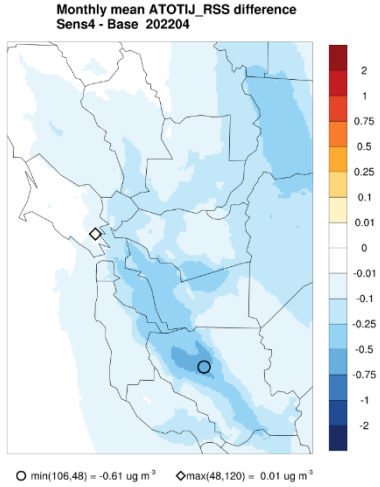

40% VOC & NOx Reduction

Figure 4-7. April average total $PM_{2.5}$ and responses to emissions reductions.

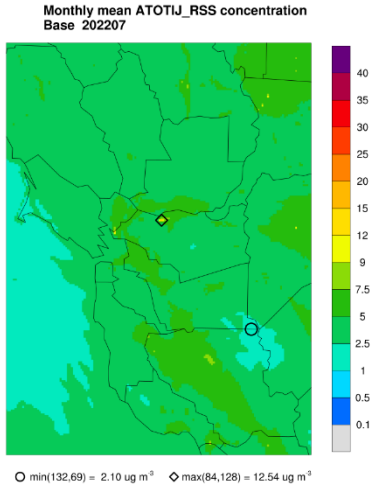

Monthly Average
Total $PM_{2.5}$

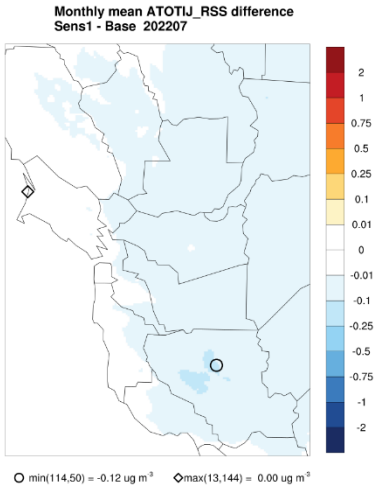

20% VOC Reduction

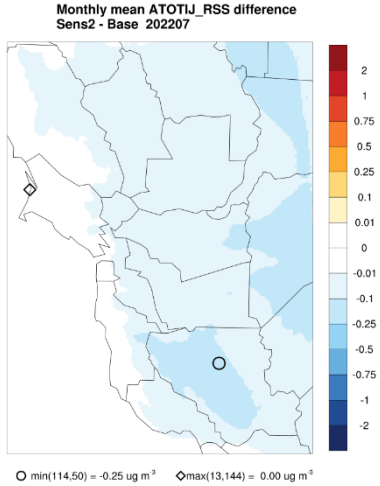

40% VOC Reduction

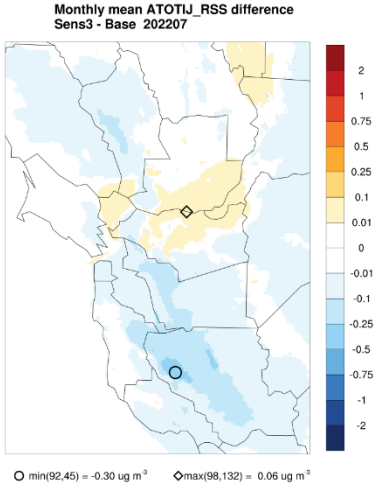

40% NOx Reduction

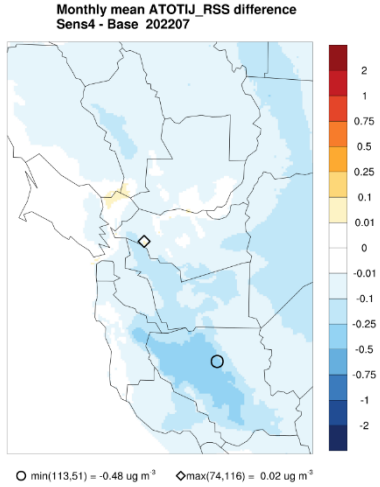

40% VOC & NOx Reduction

Figure 4-8. July average total $PM_{2.5}$ and responses to emissions reductions.

5.0 CONCLUSIONS AND RECOMMENDATIONS

The model performance evaluation for total $PM_{2.5}$ over all monitoring locations within the Air District's jurisdiction and speciated $PM_{2.5}$ at a single CSN monitor showed that using SAPRC-22 chemistry improved model performance in spring by reducing the under-prediction bias, but worsened performance in winter by increasing the over-prediction bias. In general, the results show that the SAPRC-22 chemistry mechanism tends to be more conducive to oxidant formation, particularly in winter, than the SAPRC07 chemistry mechanism used in prior Air District CMAQ applications. This is confirmed by a comparison of ozone concentrations from the SAPRC07 and SAPRC-22 simulations.

Including VCP chemistry and using MEGAN emissions instead of BEIS emissions had a negligible effect on model performance. Nevertheless, the VCP updates to CMAQ represent an improvement to the model as the importance of VCP chemistry has been noted by a number of researchers (e.g., McDonald et al., 2018; Zhu et al., 2024; Stockwell et al., 2025).

While the over-prediction bias in $PM_{2.5}$ predictions in winter worsened when using SAPRC-22 chemistry, this could be related to uncertainties in the emission inventory, particularly the VOC inventory. Other sources of uncertainty include the boundary conditions from WACCM.

Results from the emission reduction scenario simulations showed that some portions of the Bay Area are likely VOC-limited, since NOx reductions resulted in increases in anthropogenic and biogenic SOA. Responses to emission reductions were larger in the winter month than in either the spring month or the summer month. Both VOC and NOx reductions are required to decrease total $PM_{2.5}$.

We recommend the following for future work:

- Conduct a robust assessment of anthropogenic emissions inventory (both VOCs and NOx)
- Assess VCP emissions inventory
- Add more speciated ($PM_{2.5}$, VOCs) monitoring sites

6.0 REFERENCES

Carter, W.P.L, 2015. Development of a database for chemical mechanism assignments for volatile organic emissions. *J. Air & Waste Manage. Assoc.,* **65 (10)**, pp. 1171-1184. https://doi.org/10.1080/10962247.2015.1013646.

Carter, W.P.L., 2023. *Documentation of the SAPRC-22 Mechanism*. Report to the California Air Resources Board, Contract No. 21AQP011, https://intra.engr.ucr.edu/~carter/SAPRC/22/S22doc.pdf.

Carter, W.P.L., J. Jiang, Z. Wang, and K.C. Barsanti, 2025. The SAPRC atmospheric chemical mechanism generation system (MechGen). *Geosci. Model Dev*., **18**, pp. 8461–8483. https://doi.org/10.5194/gmd-18-8461-2025.

Chen, T., P. Zhang, Q. Ma, B. Chu, J. Liu, Y. Ge, and H. He, 2022. Smog chamber study on the role of NOx in SOA and O_3 formation from aromatic hydrocarbons. *Env. Sci. & Tech*. **56(19)**, pp. 13654-13663. https://doi.org/10.1021/acs.est.2c04022.

Emery, C., Z. Liu, A.G. Russell, M.T. Odman, G. Yarwood, and N. Kumar, 2017. Recommendations on statistics and benchmarks to assess photochemical model performance. *J. Air & Waste Manage. Assoc.*, **67(5)**, pp. 582-598. https://doi.org/10.1080/10962247.2016.1265027.

Gao, C., X. Zhang, L. Huang, H. Yang, H. Zhao, S. Zhang, and A. Xiu, 2025. Model intercomparisons of MEGAN and BEIS: Synergistic impacts of biogenic VOCs and soil NO emissions on summer ozone and secondary organic aerosol formation in China. *ACS EST Air*, **2(8)**, pp. 1538–1551. https://doi.org/10.1021/acsestair.5c00038.

Guenther, A., J. Campos, P. Harley, X. Jiang, S. Kim, A. Mielnik, S. Nagalingham, J. Ortega, Y. Zhang, T. Shah, L. Huang, and G. Yarwood, 2019. *Next Steps for improving Texas Biogenic VOC and NO Emission Estimates* (AQRP Project 18-005). Prepared for the Texas Air Quality Research Program, by University of California at Irvine and Ramboll, October 2019. https://aqrp.ceer.utexas.edu/edocman/projectinfoFY18_19/18-005/18-005%20Final%20Report.pdf.

Guenther, A., Y. Zhang, H. Wang, S. Nagalingam, and V.M. Ruiz, 2025. *San Francisco Bay Area BVOC Emissions Project Final Report*. Prepared for the Bay Area Air Quality Management District by University of California at Irvine, September 2025. Available from the Air District by request.

Hallward-Driemeier, A.H., J.R. Hall, K.A. Spence, B.P. Telicki, A.F. Schaeffer, J.C. Avila, I.S. Albores, and A.J. Carrasquillo, 2024. Secondary organic aerosol formation and chemistry from the OH-initiated oxidation of monofunctional C10 species. *ACS Earth and Space Chemistry,* **8(5)**, pp. 907-919. https://doi.org/10.1021/acsearthspacechem.3c00180.

Hogrefe, C., S.S. Isukapalli, X., Tang, P.G. Georgopoulos, S. He, E.E. Zalewsky, W. Hao, J.-Y. Ku, T. Key, and G. Sistla, 2011. Impact of biogenic emission uncertainties on the simulated response of ozone and fine particulate matter to anthropogenic emission reductions. *J. Air Waste Manage. Assoc.*, **61(1)**, pp. 92–108. https://doi.org/10.3155/1047-3289.61.1.92.

Karamchandani, P., K. Tuite, P. Vennam, and G. Yarwood, 2025. *Implementation of the SAPRC-22 Mechanism in CMAQv5.4*. Prepared for the U.S. EPA under Task Order 68HERD21A0002, Contract

No. 68HERH24F0296. https://github.com/USEPA/CMAQ/blob/5.4_SAPRC22/DOCS/SAPRC22_Report_Deliverable_3.4.25.V2.pdf.

Kroll, J.H., N.L. Ng, S.M. Murphy, R.C. Flagan, and J.H. Seinfeld, 2006. Secondary organic aerosol formation from isoprene photooxidation. *Env. Sci. & Tech*. **40(6)**, pp. 1869-1877. https://doi.org/10.1021/es0524301.

Lane, T.E., N.M. Donahue, and S.N. Pandis, 2008. Effect of NOx on Secondary Organic Aerosol Concentrations. *Env. Sci. & Tech*. **42(16)**, pp. 6022-6027. https://doi.org/10.1021/es703225a.

Li, W., Li, L., Chen, C.L., Kacarab, M., Peng, W., Price, D., Xu, J. and Cocker III, D.R., 2018. Potential of select intermediate-volatility organic compounds and consumer products for secondary organic aerosol and ozone formation under relevant urban conditions. *Atmos. Environ*. **178**, pp.109-117. https://doi.org/10.1016/j.atmosenv.2017.12.019.

Li, K., J. Liggio, C. Han, Q. Liu, S.G. Moussa, P. Lee, and S-M. Li, 2019. Understanding the impact of high-NOx conditions on the formation of secondary organic aerosol in the photooxidation of oil sand-related precursors. *Env. Sci. & Tech*. **53(24)**, pp. 14420-14429. https://doi.org/10.1021/acs.est.9b05404.

Liu, S., X. Xu, S. Zhang, R. Li, Z. Li, C. Wu, R. Li, F. Chen, G. Zhang, and G. Wang, 2025. Changes in gas-to-aerosol-phase partitioning ratio of semi-volatile products affect secondary organic aerosol formation from α-pinene photooxidation. Atmos. Environ. **360**, 121427. https://doi.org/10.1016/j.atmosenv.2025.121427.

Lu, Q., B.N. Murphy, M. Qin, P.J. Adams, Y. Zhao, H.O. Pye, C. Efstathiou, C. Allen, and A.L. Robinson, 2020. Simulation of organic aerosol formation during the CalNex study: updated mobile emissions and secondary organic aerosol parameterization for intermediate-volatility organic compounds. *Atmos. Chem. Phys*. **20**, pp. 4313-4332. https://doi.org/10.5194/acp-20-4313-2020.

McDonald, B.C., J.A. de Gouw, J.B. Gilman, S.H. Jathar, A. Akherati, C.D. Cappa, J.L. Jimenez, J. Lee-Taylor, P.L. Hayes, S.A. McKeen, Y.Y. Cui, S.-W. Kim, D.R. Gentner, G. Isaacman-VanWertz, A.H. Goldstein, R.A. Harley, G.J. Frost, J.M. Roberts, T.B. Ryerson, and M. Trainer, 2018. Volatile chemical products emerging as largest petrochemical source of urban organic emissions. *Science*, **359**, pp. 760-764. https://www.science.org/doi/10.1126/science.aaq0524.

Ng, N.L., J.H. Kroll, A.W.H. Chan, P.S., Chhabra, R.C., and J.H. Seinfeld, 2007a. Secondary organic aerosol formation from m-xylene, toluene, and benzene. *Atmos. Chem. Phys*., **7**, pp. 3909–3922, https://doi.org/10.5194/acp-7-3909-2007, 2007.

Ng, N. L., P.S. Chhabra, A.W.H. Chan, J.D. Surratt, J.H. Kroll, A.J. Kwan, D.C. McCabe, P.O. Wennberg, A. Sorooshian, S.M. Murphy, N.F. Dalleska, R.C. Flagan, and J.H. Seinfeld, 2007b. Effect of NOx level on secondary organic aerosol (SOA) formation from the photooxidation of terpenes, *Atmos. Chem. Phys*., **7**, pp. 5159–5174. https://doi.org/10.5194/acp-7-5159-2007.

Pennington, E.A., K.M. Seltzer, B.N. Murphy, M. Qin, J.H. Seinfeld, and H.O. Pye, 2021. Modeling secondary organic aerosol formation from volatile chemical products. *Atmos. Chem. Phys*., **21**, pp. 18247-18261. https://doi.org/10.5194/acp-21-18247-2021.

Pfannerstill, E.Y., C. Arata, Q. Zhu, B.C. Schulze, R. Ward, R. Woods, C. Harkins, R.H. Schwantes, J.H. Seinfeld, A. Bucholtz, R.C. Cohen, and A.H. Goldstein, 2024. Temperature-dependent emissions dominate aerosol and ozone formation in Los Angeles. *Science,* **384**, pp. 1324–1329. https://www.science.org/doi/10.1126/science.adg8204.

Pullinen, I., S. Schmitt, S. Kang, M. Sarrafzadeh, P. Schlag, S. Andres, E. Kleist, T.F. Mentel, F. Rohrer, M. Springer, R. Tillmann, J. Wildt, C. Wu, D. Zhao, A. Wahner, and A. Kiendler-Scharr, 2020. Impact of NOx on secondary organic aerosol (SOA) formation from α-pinene and β-pinene photooxidation: the role of highly oxygenated organic nitrates. *Atmos. Chem. Phys*., **20**, pp. 10125–10147. https://doi.org/10.5194/acp-20-10125-2020.

Sasidharan, S., Y. He, A. Akherati, Q. Li, W. Li, D. Cocker, B.C. McDonald, M.M. Coggon, K.M. Seltzer, H.O. Pye, J.R. Pierce, and S.H. Jathar, 2023. Secondary organic aerosol formation from volatile chemical product emissions: model parameters and contributions to anthropogenic aerosol. *Env. Sci. & Tech*. **57**, pp. 11891-11902. https://doi.org/10.1021/acs.est.3c00683.

Seltzer, K.M., E. Pennington, V. Rao, B.N. Murphy, M. Strum, K.K. Isaacs, and H.O. Pye, 2021. Reactive organic carbon emissions from volatile chemical products. *Atmos. Chem. Phys*., **21**, pp. 5079–5100. https://doi.org/10.5194/acp-21-5079-2021.

Song, C., K. Na, and D.R. Cocker, 2005. Impact of the hydrocarbon to NOx ratio on secondary organic aerosol formation. *Env. Sci. & Tech*. **39(9)**, pp. 3143-3149. https://doi.org/10.1021/es0493244.

Stockwell, C.E., M.M. Coggon et al., 2025. Urban ozone formation and sensitivities to volatile chemical products, cooking emissions, and NOx upwind of and within two Los Angeles Basin cities. *Atmos. Chem. Phys*., **25**, pp. 1121–1143. https://doi.org/10.5194/acp-25-1121-2025.

Wang, S., N.T. Tsona, and L. Du, 2021. Effect of NOx on secondary organic aerosol formation from the photochemical transformation of allyl acetate. *Atmos. Environ*., **255**, 118426. https://doi.org/10.1016/j.atmosenv.2021.118426.

Wang, Z., F. Couvidat, and Karine Sartelet, 2024. Response of biogenic secondary organic aerosol formation to anthropogenic NOx emission mitigation. *Science of The Total Environment*, **927**, 172142. https://doi.org/10.1016/j.scitotenv.2024.172142.

Wei, D., C. Cao, A. Karambelas, J. Mak, A. Reinmann, R. Commane, 2024. High-resolution modeling of summertime biogenic isoprene emissions in New York City. *Environ. Sci. Technol*., **58(31)**, pp. 13783–13794. https://doi.org/10.1021/acs.est.4c00495

Yarwood, G. and K. Tuite, 2024. Representing ozone formation from volatile chemical products (VCP) in Carbon Bond (CB) chemical mechanisms. *Atmosphere***, 15 (2)**, 178. https://doi.org/10.3390/atmos15020178.

Zhu, Q., R.H. Schwantes et al., 2024. A better representation of volatile organic compound chemistry in WRF-Chem and its impact on ozone over Los Angeles. *Atmos. Chem. Phys*., **24**, pp. 5265–5286. https://doi.org/10.5194/acp-24-5265-2024.